

OPEN ACCESS

Efficient Workflows for Detecting Li Depositions in Lithium-Ion Batteries

To cite this article: Thomas Waldmann *et al* 2024 *J. Electrochem. Soc.* **171** 070526














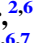



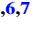


View the [article online](#) for updates and enhancements.

You may also like

- [In Situ Optical Investigations of Lithium Depositions on Pristine and Aged Lithium Metal Electrodes](#)
Hannes Kühnle, Edwin Knobbe and Egbert Figgemeier
- [Temperature-Adaptive Alternating Current Preheating of Lithium-Ion Batteries with Lithium Deposition Prevention](#)
Hao Ge, Jun Huang, Jianbo Zhang et al.
- [In Situ Atomic Force Microscopy Study on Lithium Deposition on Nickel Substrates at Elevated Temperatures](#)
Ryo Mogi, Minoru Inaba, Yasutoshi Iriyama et al.



Efficient Workflows for Detecting Li Depositions in Lithium-Ion Batteries

Thomas Waldmann,^{1,2,z}  Christin Hogrefe,¹  Marius Flügel,¹  Ivana Pivarníková,^{3,4} 
 Christian Weisenberger,⁵  Estefane Delz,⁵  Marius Bolsinger,⁵  Lioba Boveleth,^{2,6} 
 Neelima Paul,³  Michael Kasper,¹  Max Feinauer,¹  Robin Schäfer,¹  Katharina Bischof,¹ 
 Timo Danner,^{2,6}  Volker Knoblauch,⁵  Peter Müller-Buschbaum,⁴  Ralph Gilles,³ 
 Arnulf Latz,^{2,6,7}  Markus Hölzle,¹  and Margret Wohlfahrt-Mehrens^{1,2} 

¹Zentrum für Sonnenenergie- und Wasserstoff-Forschung (ZSW), D-89081 Ulm, Germany

²Helmholtz Institute Ulm for Electrochemical Energy Storage (HIU), D-89081 Ulm, Germany

³Technical University of Munich, Heinz Maier-Leibnitz-Zentrum (MLZ), D-85748 Garching, Germany

⁴Technical University of Munich, TUM School of Natural Sciences, Department of Physics, Chair for Functional Materials, 85748 Garching, Germany

⁵Aalen University of Applied Sciences (AU), Materials Research Institute, D-73430 Aalen, Germany

⁶German Aerospace Center (DLR), Institute of Engineering Thermodynamics, D-70569 Stuttgart, Germany

⁷Ulm University (UUlm), Institute of Electrochemistry, D-89081 Ulm, Germany

Lithium deposition on anode surfaces can lead to fast capacity degradation and decreased safety properties of Li-ion cells. To avoid the critical aging mechanism of lithium deposition, its detection is essential. We present workflows for the efficient detection of Li deposition on electrode and cell level. The workflows are based on a variety of complementary advanced physico-chemical methods which were validated against each other for both graphite and graphite/Si electrodes: Electrochemical analysis, scanning electron microscopy, glow discharge-optical emission spectroscopy and neutron depth profiling, ex situ optical microscopy, in situ optical microscopy of cross-sectioned full cells, measurements in 3-electrode full cells, as well as 3D microstructurally resolved simulations. General considerations for workflows for analysis of battery cells and materials are discussed. The efficiency can be increased by parallel or serial execution of methods, stop criteria, and design of experiments planning. An important point in case of investigation of Li depositions are rest times during which Li can re-intercalate into the anode or react with electrolyte. Three workflows are presented to solve the questions on the occurrence of lithium deposition in an aged cell, the positions of lithium deposition in a cell, and operating conditions which avoid lithium depositions in a cell.

© 2024 The Author(s). Published on behalf of The Electrochemical Society by IOP Publishing Limited. This is an open access article distributed under the terms of the Creative Commons Attribution 4.0 License (CC BY, <http://creativecommons.org/licenses/by/4.0/>), which permits unrestricted reuse of the work in any medium, provided the original work is properly cited. [DOI: 10.1149/1945-7111/ad5ef8]



Manuscript received March 5, 2024. Published July 15, 2024.

Supplementary material for this article is available [online](#)

Increased sustainability and reduced dependency on foreign critical resources (e.g. Co and Li) go hand in hand with increased cycle life and second use of aged Li-ion batteries. The usable lifetime of Li-ion batteries is limited by aging mechanisms on the material, electrode, and cell level.^{1–10} Known aging mechanisms on the anode side include continued growth of the solid-electrolyte interphase (SEI) on graphite anodes,^{1,4,11–15} degradation of the Si component in graphite/Si anodes,^{16–22} transition metal dissolution from the cathode and migration to the anode,^{23–26} as well as electrode deformations.^{5,6,27–32}

Li deposition on graphite and graphite/Si anodes is a critical aging mechanism that leads to rapid capacity degradation by reaction of deposited metallic Li with electrolyte and formation of electronically insulated “dead Li.”^{8,11,17,18,24,33–45} Li depositions can even reduce the safety level (internal short circuit due to Li dendrites and exothermic reactions with the electrolyte).^{8,40,46–51} For example under the quasi-adiabatic conditions during accelerated rate calorimetry (ARC) experiments, the onset of self-heating (indicating exothermic reactions) and the onset of thermal-runaway was significantly reduced for cells with Li plating compared to fresh and aged cells without Li depositions.^{46,47,49}

Li deposition on negative electrodes often occurs during fast charging, at low temperatures, and at high states-of-charge (SOC).^{8,10,17,33–35,37,38,45,52–57} In particular in case of graphite/Si anodes, degradation of the Si component (loss of anode active material^{18,58}) during aging can also lead to increased susceptibility of a cell to Li deposition.¹⁸ In case clogging of the anode pores

occurs during aging, Li deposition can also happen in later stages of aging.⁵⁹

Although these are general trends, the exact operating conditions to avoid Li deposition need to be determined for each cell type.^{34,35,45} Post-Mortem analysis shows that there is a difference between Li deposition (generic term) happening at low temperature charging even at moderate C-rates (homogeneous Li plating) and at high temperature charging with high C-rates (local Li deposition).⁸

In literature, there is a variety of physico-chemical methods to detect Li deposition on anodes of Li-ion batteries, while most methods rather provide hints than evidence for this degradation mechanism.^{8,33,36,46–48,53–56,60–69} The existing techniques can be divided into electrochemical,^{8,33–35,41,45,46,53,56,57,60–63,69–75} ex situ,^{18,35,36,48,65–67,69,75–80} in situ,^{20,68,69,75,81–84} and operando^{17,54–56,60,64,69,75,85} methods. Paul et al. recently divided the available methods into global vs local, direct vs indirect, as well as quantitative vs qualitative.⁶⁹

Simulations of Li depositions have been performed in full cells with 3D microstructurally resolved electrode models,^{86–89} pseudo-3D,^{90–92} pseudo-2D,^{39,59,89,93–104} and 1D models,^{105–107} as well as by first-principles calculations.^{108–110} Validated electrochemical models, or digital twins of the battery cell, are able to predict if and where in a cell Li deposition occurs. Therefore, simulations support experimental characterization methods.

However, there is still a need for efficient workflows (WF) with combination of various physico-chemical methods to increase the trustworthiness of the results. A WF can be defined as a spatial and temporal sequence of interrelated operations.^{111,112} In general, WFs can increase efficiency by planning tasks (especially if they are repetitive), minimizing time and costs. In a chemical analytical pathway, the WF covers the sample preparation and handling, as

^zE-mail: thomas.waldmann@zsw-bw.de

well as the sequence of the methods to be applied and data evaluation.

The applied methods in a WF must

- (1) complement and balance each other's strengths and weaknesses. Using methods with different measurement principles can help to identify and avoid systematic errors.
- (2) deliver reliable results, i.e. the results of each method must be reproducible with the same method.
- (3) be validated against each other.

For example, we recently performed a method validation for voltage relaxation, glow discharge optical emission spectroscopy (GD-OES) depth profiling, and optical microscopy (OM),³⁵ as well as for GD-OES and neutron depth profiling (NDP) resulting in a very high benefit of sample characterization.¹¹³

By using complementary methods, possibly in combination with data-driven or simulation-based techniques, analysis results can be made more efficient and reliable. The specific WF depends on the scientific question. Existing WF-like descriptions focus on cell disassembly and Post-Mortem analysis,^{7,29} as well as development of charging procedures.^{114,115} However, in case of the detection of Li depositions on anodes in Li-ion batteries, no WF is available in literature so far.

In the present paper, we firstly give insights into battery characterization WFs in general. Secondly, the considered characterization methods and their validation are described briefly. Finally, we present three WFs on the questions of (i) the occurrence of Li deposition in an aged cell, (ii) the positions of Li deposition in a cell, and (iii) operating conditions which avoid Li depositions in an aged cell.

General Considerations for Battery Characterization Workflows

This section describes WFs for characterization of battery cells and materials in general and for Li depositions in particular.

Figure 1 shows two basic general characterization WFs. The characterization techniques depicted in Fig. 1a are implemented sequentially. A sequential WF allows to decide if more tests are required after each measurement. The methods 1 to n can be arranged within the WF by increasing efforts, i.e. costly measurements (often giving more insights) might not be necessary if previous results have already delivered the information needed. For example, ex situ OM is a less expensive method (e.g. no pumps and high vacuum needed) compared with X-ray photoelectron spectroscopy (XPS). However, OM also provides much less insights compared with XPS. Consequently, the serial approach (e.g. OM → XPS) has the potential to be more cost effective, since less effort might be needed to get a sufficient result. On the other hand, application of different methods in series and the decisions in between the application of the characterization methods is usually

more time consuming than applying the methods in parallel. Another possibility to determine the sequence of characterization methods in a WF is starting with broad-spectrum methods to get a general overview of the sample and more specific insights by subsequent measurements.

Figure 1b depicts a potentially faster WF, where the methods are applied in parallel. In more complex characterization WFs, some methods might be also carried out in parallel, while others are in series. One reason for conducting parallel measurements is the complementarity of methods, which enhances the reliability of the results.

The time needed to perform measurements can be very diverse for different methods. For example, while the observation of Li depositions with OM can be performed in several minutes, a GD-OES measurement to analyze the Li content in an electrode takes several hours since a crater has to be sputtered into the sample and more evaluation time is required. To take this into account in time-optimized WFs, a sequence of different fast methods (or a lot of measurements with one fast method) might be performed in series, while at the same time measurements with slow methods are conducted in parallel.

The samples can generally either be complete battery cells (electrochemical or other non-destructive tests) or material samples (anode, cathode, separator, or electrolyte) obtained from disassembly (Post-Mortem analysis) of a cell. In case the same samples are used for subsequent measurements, it must be considered that previous methods are not destructive. Further considerations are how many samples have to be taken and how homogeneous the samples are.

Due to possible relaxation processes^{17,46,55,56,62,116–120} in the electrodes, rest periods must be well considered. Especially in the case of Li depositions, re-intercalation into graphite and alloying with Si of the anode is likely to happen.^{46,55,56,62,117} In case the rest time between the end of cycling and disassembly is too long, a part of the reversibly deposited Li could re-intercalate into graphite.^{8,47,55,56,62,68,117} This was observed in voltage relaxation curves which were recorded directly after the end of constant current charging during neutron diffraction for graphite anodes in commercial cells,⁵⁶ for graphite/Si anodes in commercial cells,¹⁷ in situ measurements of cross-sectioned full cells,⁶⁸ as well as in experiments of Li metal which was pressed on a graphite electrode surface (for example see Fig. 2a and video S1 in supporting information).^{117,121,122} In Post-Mortem experiments of cells with Li plating, where disassembly was carried out directly after the end of cycling and after a rest time of 8 days at 25 °C clear differences were observed: (i) The Li peak in GD-OES measurements was lower and broader (compare Figs. 2b, 2c), (ii) the anode appeared less shiny and more grayish (compare insets of Figs. 2b, 2c), and (iii) the film covering the graphite particles appeared not dendritic anymore in scanning electron microscopy (SEM) measurements (compare Figs. 2d, 2e).⁴⁷

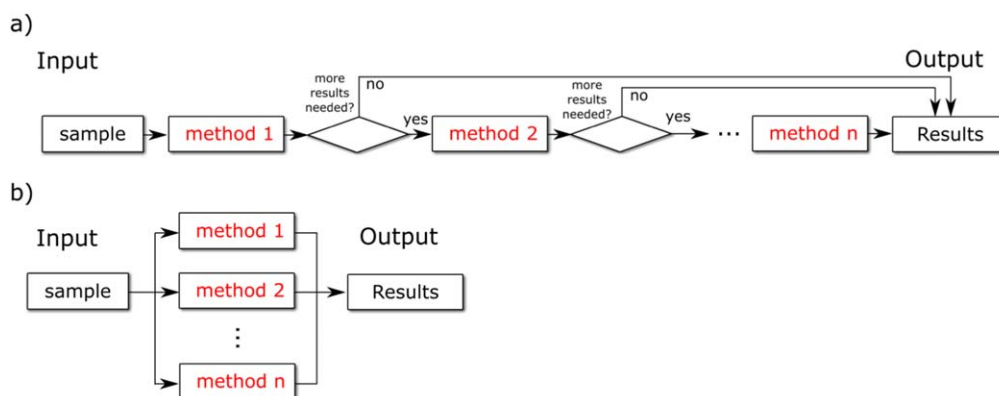


Figure 1. Basic WFs defining the sequence of n methods applied on a sample for (a) serial and (b) parallel characterization. For the specific WFs on detection of Li depositions below the methods are in parallel, however, they could in principle be also in series.

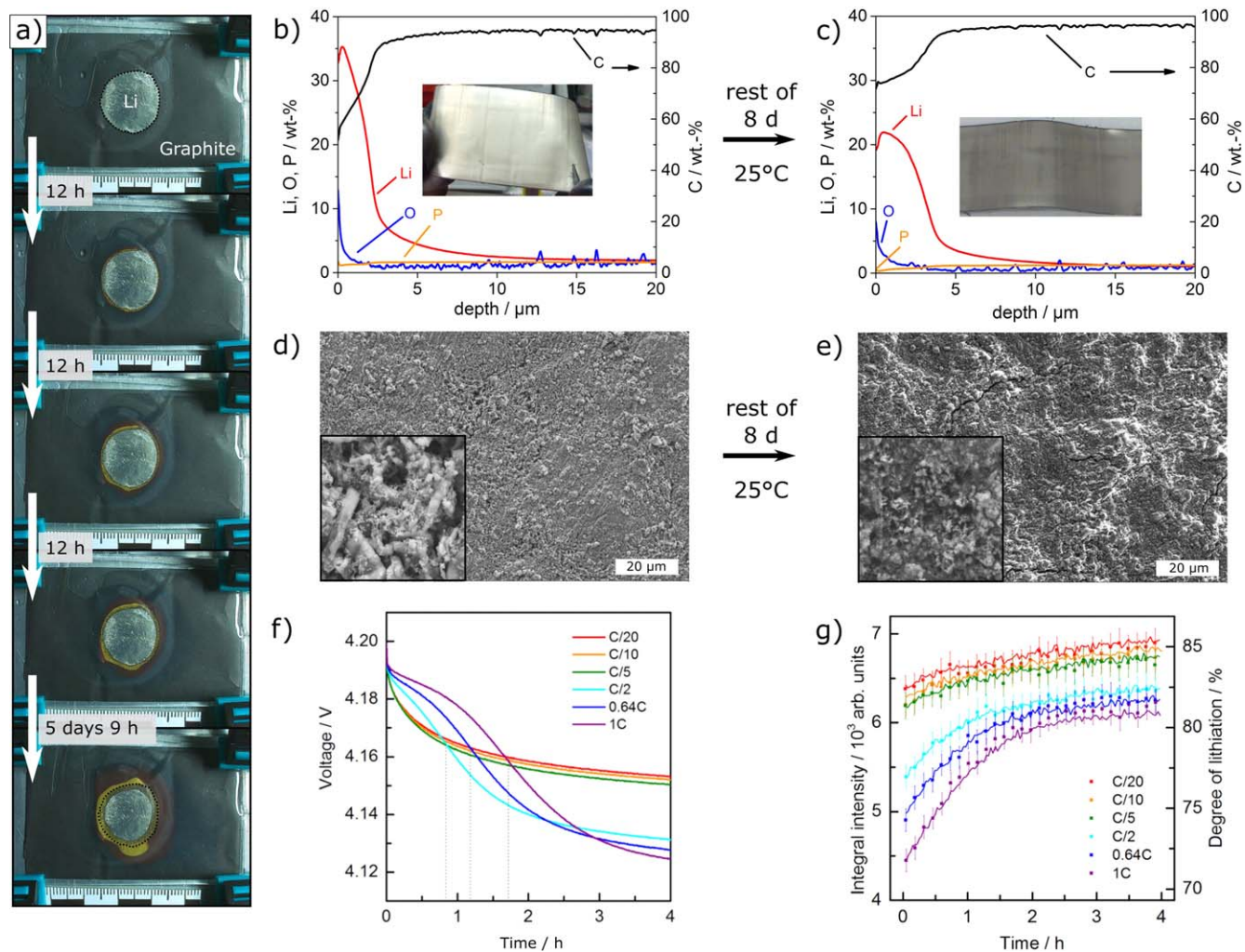


Figure 2. (a) Li metal pressed against a graphite anode after the given rest times.¹¹⁷ (b), (c) GD-OES and (d)–(e) SEM measurements of anodes taken from commercial 18650 cells after cycling under Li plating conditions.⁴⁷ The insets in (b), (c) show photographs of the anodes directly after cell disassembly.⁴⁷ The insets in (d), (e) show magnifications with $6 \times 6 \mu\text{m}^2$.⁴⁷ (b), (d) Cell disassembly directly after the end of cycling and (c), (e) disassembly after 8 days of rest at 25 °C.⁴⁷ Simultaneously measured voltage relaxation (f) and integral intensity of LiC₆ in operando neutron diffraction experiments at the STRESS-SPEC instrument (g).⁵⁶ (f) and (g) use the same color code. (a) Reprinted with permission from Ref. 117, (b)–(e) modified with permission from Ref. 47, (f), (g) reprinted with permission from Elsevier from Ref. 56 Copyright Elsevier.

Exemplary measurements of voltage relaxation after charging are shown in Fig. 2f.⁵⁶ If Li deposition is present on the anode after charging, the beginning of the voltage relaxation curve is dominated by a mixed potential.^{62,63} In case a part of the deposited Li is reversible, re-intercalation will happen and the mixed potential changes towards the potential of the pure anode without Li.⁶² This leads to a different shape of the voltage relaxation curve.⁶² In Fig. 2f, this is the case for charging rates ≥ 0.5 C (light blue, blue, and purple curves). In contrast, the voltage relaxation curves after charging at C-rates < 0.5 C (green, orange, and red curves) have a steadily declining shape indicating no Li depositions.⁵⁶ Others observed the same trends and similar curve shapes for other cell types.^{17,35,114}

Figure 2g shows changes of the LiC₆ integral intensity in operando neutron diffraction experiments with the STRESS-SPEC instrument (same colors as in Fig. 2f).⁵⁶ For < 0.5 C (green, orange, and red data points), the integral intensities undergo only minor increases, whereas for ≥ 0.5 C (light blue, blue, and purple data points) a significantly higher non-linear increase is observed.⁵⁶ The operando neutron diffraction experiments with graphite anodes (Fig. 2g) are in full accordance with the voltage relaxation of the same cell (Fig. 2f)⁵⁶ and with earlier neutron scattering results by Zinth et al.⁵⁵

If deposited Li is re-intercalating during a rest time into graphite/Si anodes, the mechanism differs slightly.¹⁷ Li is mostly intercalating

into graphite first (and most likely also in parallel alloying with the Si compound) and is then rearranged from graphite into the Si compound.¹⁷ In neutron diffraction experiments, this is observed by an increase of the LiC₆ integrated intensity (as for graphite anodes without Si^{55,56}) followed by a decrease of the LiC₆ integrated intensity (due to the presence of the Si compound).¹⁷ Interestingly, the change of the LiC₆ integrated intensity from neutron diffraction experiments coincides with the turning point of the differential voltage curve of the simultaneously measured voltage curves.¹⁷

Additionally, ARC experiments performed directly after the end of cycling under Li plating conditions showed significantly different onset temperatures (~ 35 °C) compared to ARC tests performed after ≥ 8 days of rest time (~ 75 °C, near the level of fresh cells).⁴⁶ In this rest time, deposited Li partly re-intercalates into graphite and reacts with electrolyte.⁴⁶

Spontaneous intercalation of Li adatoms into highly oriented pyrolytic graphite (HOPG) surfaces was also observed in surface science experiments.^{118–120,123} Density functional theory (DFT) calculations showed that the barriers for Li crossing a defect-free graphene plane through a C₆ ring are as high as 10.2 eV, however, this barrier is reduced by defects (e.g. 2.36 eV for a divacancy).¹²⁴ The high barrier makes it unlikely that Li intercalates through a defect-free basal plane into graphite. In contrast, the mobility of Li

adsorbed on a clean graphene surface is high due to the low diffusion barrier which is in the range of $\sim 0.2\text{--}0.4$ eV as predicted by DFT calculations.^{125,126} Mandelkort et al. determined an activation barrier of (0.16 ± 0.02) eV for intercalation of Li from a HOPG surface into HOPG.¹²³ The authors claimed that Li intercalation into graphite bulk most likely takes place at defects and step edge sites of the HOPG basal plane, which are reached via Li surface diffusion.¹²³ In contrast to HOPG in ultra-high vacuum, the presence of a SEI layer and of liquid electrolyte has to be considered. In graphite particles, the re-intercalation of deposited Li metal likely takes place at defects and edge sites of the basal plane and through the edge plane.

In accordance with this, Li metal pressed against a graphite anode (Fig. 2a) leads to dissolution of Li and lithiation of graphite.¹¹⁷ This reaction happens even without electrolyte, however it is much faster with electrolyte.¹¹⁷ In model cells and simulations with a graphite anode in contact with Li metal against a Li counter electrode, it was found that the minimum of the potential in the relaxation corresponds to the point in time when the Li is completely dissolved.¹¹⁷

All these results from complementary methods show the importance of considering the influence of rest periods in case of samples with Li depositions. We stress that it is very important for all WFs to know and control the time between the end of cycling and the beginning of the cell disassembly, because re-intercalation and reaction of Li with electrolyte will reduce the amount and morphology of detectable Li metal. In some cases this might be difficult, e.g. for aged batteries from an application in the field. However, also in such cases, the possibility of re-intercalating or reacting Li has to be considered.

When samples are taken from disassembled cells, they are often washed to reduce remaining electrolyte conductive salt (mostly LiPF₆) and prevent corrosion issues.^{7,11,12,42,76,127–136} On the other hand, one has to keep in mind that soluble components, e.g. a part of the SEI will also be removed by the washing procedure.¹²⁷ Therefore sample washing should be carried out in a defined and reproducible way to allow comparability.⁷ Dimethyl carbonate (DMC) is most commonly used for sample washing.^{7,11,12,42,76,127–136} Some authors apply extensive washing,^{11,12} while others chose dip washing^{34,127} (e.g. 2 min in DMC¹²⁷), and others do not wash their samples.^{7,33,42,52,53,137,138} The omission of sample washing^{7,33,42,52,53,137,138} retains not only the soluble compounds but also the residual LiPF₆ in the samples. In case of samples with Li deposition, washing with DMC will most likely not wash away Li metal. Instead, metallic Li will react with DMC and the soluble parts of existing SEI will be affected.

The high reactivity of Li depositions with N₂, O₂, CO₂, and H₂O has also implications for sample preparation and handling. The reaction of Li is not only affected thermodynamically by the low redox potential of Li/Li⁺ vs SHE of -3.045 V,¹³⁹ but also by the high specific surface area of mostly dendritically deposited Li.^{8,35,36,47,66–68,72,109,110,140–147} Safety precautions must be taken when handling anode samples with Li deposition, because Li depositions from cells in contact with water can cause fire.⁴⁰

Otto et al. characterized the passivation layers on differently prepared and stored Li metal samples by energy dispersive X-ray spectroscopy (EDX), XPS, and time-of-flight secondary ion mass spectrometry (ToF-SIMS).¹⁴⁸ Their measurements indicate a bilayered structure composed of a hydroxide layer and carbonate on top of an oxide-rich layer which is in contact with Li metal.¹⁴⁸ The thickness and composition of the surface passivation layers on Li metal depend on the preparation, storage, and transport conditions of the samples.¹⁴⁸ The authors showed that storage in a glovebox is not sufficient to fully prevent sample changes during a storage time of 2 weeks.¹⁴⁸ Therefore, the authors recommend storing Li metal containing samples in sealed pouch bags, even in Ar-filled glove boxes when a storage time of one day is exceeded.¹⁴⁹ In Ar-filled glove boxes, p(H₂O), p(O₂), and p(N₂) should be controlled.¹⁴⁹ N₂-filled glove boxes are not recommended due to the reaction with Li to Li₃N. While very thin passivation layers might be only detectable by surface sensitive methods such as ToF-SIMS and

XPS, air contact of samples has most likely no large effect on SEM observations, where the form of dendritic structure is often still maintained.^{35,36,47} However, if anode samples with Li depositions get into contact with air, it must be considered that the observed dendritic structures are not Li metal but most likely Li oxides or hydroxides.

Most EDX devices are not capable to detect Li. However, recent progress in windowless silicon drift detectors (SDD) allows to detect the low energy X-rays needed for Li detection. Hovington et al. showed that Li K α lines can be detected by EDX using a windowless detector from Oxford Instruments.¹⁵⁰ Recent studies showed, that this technique can also be used for a quantitative analysis of Li.^{151,152} For standard EDX detectors an intentional exposure of anodes samples with Li deposition to air can have an advantage in EDX: If Li reacts with oxygen, the reaction product is enriched with oxygen which can then be detected by EDX giving a hint on Li deposition.^{36,113}

When samples are transported or shipped to other measuring facilities within a WF, it is important to pay attention to the packaging. Not only the airtightness is important, however also the mechanical properties. Li is one of the softest metallic materials with the highest ductility.^{153,154} Therefore we recommend placing the samples in a container that cannot be compressed from outside. Additionally, if samples are transported by parcel shipping, dangerous goods regulations for the transport of the respective chemicals must be followed.

Additionally, the minimum material amount needed for each analysis method has to be considered. When aging mechanisms are analyzed, it is good practice to compare the results from aged cells with fresh cells that can be expected to be not affected by aging mechanisms.⁷ The fresh cells provide a baseline, e.g. in terms of the amount of irreversibly trapped Li in the anode.

Deviations from an ideal WF cause frictions, leading to delays and in the worst case to measurements which have to be repeated. For a WF with the lowest possible friction, sample labeling and excellent communication are essential.

Method Selection for Detection of Li Depositions in Efficient Workflows

A distinction of methods can be made between simple methods (with rather low cost and low preparation effort) and advanced methods that offer added value. Some methods rather provide hints on Li deposition (e.g. observation of dendritic structures on the sample surface), while other methods deliver evidence (e.g. confirmation of metallic Li present in the sample). On the other hand, the combination of a critical amount of hints might be adequate to be sufficiently sure about the presence of Li depositions on an anode.

Since each method can only be used to observe certain aspects of the sample properties, a combination of complementary methods is very advantageous.^{7,155} Examples are surface/bulk sensitive methods, different resolutions of methods, or the proximity of a setup to real cells. It also has to be considered in a WF with multiple methods which provide hints on Li depositions that the combination of results from several methods can make the result more reliable. Furthermore, techniques can be divided into qualitative, semi-quantitative, and quantitative methods.

A variety of methods for investigation of Li depositions is available in literature.^{69,75} In this review, we focus on the methods available in our consortium which were validated against each other and deliver reproducible results on Li deposition (see Table I and Fig. 3 for overview). However, some of the methods discussed in the present paper might be exchanged by other methods, such as ⁷Li NMR,^{80,156,157} dilatometry,^{54,64} multi-directional laser scanning,¹⁵⁸ as well as ultrasound¹⁵⁹ after their validation. We note that implementing other methods in an existing WF requires work, such as validation by complementary methods with the same samples.

As shown in Fig. 3, the selected methods in WF 1–3 include surface sensitive (OM, SEM, EDX), cross-sectional (IOM), depth

Table I. Overview on physico-chemical and electrochemical methods for detection of Li depositions which were considered in this review.

#	Method	Detection principle	Surface/bulk/cell	Chemical/electrochemical detection of Li	WF	Type of result	References
1	GD-OES	Sample sputtering in Ar plasma, detection by OES, semi-quantitative evaluation of deposited Li amount	surface/bulk (depth profiling)	yes	1–3	evidence	18,35,36,47,76,78,113
2	NDP	Non-destructive, isotope sensitive nuclear technique to quantitatively probe depth specific concentration profiles of specific elements, such as Li, from the residual energy spectrum of emitted charged particles	surface/bulk (depth profiling)	yes	1–3	evidence	113,168,172,173,175,196–198
3	IOM	In situ optical microscopy of cross-sectioned full cell, color change of lithiated graphite and direct observation of Li depositions	surface/bulk (cross-sectioned cell)	no	2	strong hint	68,178,181
4	OM	Dendritic structures on μm scale	surface	no	1–3	hint	35
5	SEM	Dendritic structures on μm scale	surface	no	1–3	hint	35,36,47,66,67
6	EDX	Reaction of deposited Li with oxygen/air and subsequent detection of oxygen by EDX	surface	no	1–3	hint	36,113
7	3-electrode cells	Measurement of anode potential vs Li/Li^+ in 3-electrode full cell	surface	yes (condition: anode potential $<0\text{ V vs Li/Li}^+$)	3	evidence	34,40,195
8	Simulation	Calculation of amount and spatial distribution of plated Li	surface/bulk	simulation	2,3	evidence	86,88,89,92,98,100
9	Voltage relaxation (after charging)	Tracking of the cell voltage in the relaxation phase after charging	cell	no	3	hint	18,56,62,72
10	Voltage (discharge curve)	Tracking of the cell voltage during (slow) discharging to observe possible plateaus	cell	no	1–3	hint	46,47,52,61
11	Arrhenius analysis	Arrhenius plots of aging rates; Li plating is indicated by higher aging rates for lower temperatures	cell	no	3	strong hint	11,37,38,45,50,195

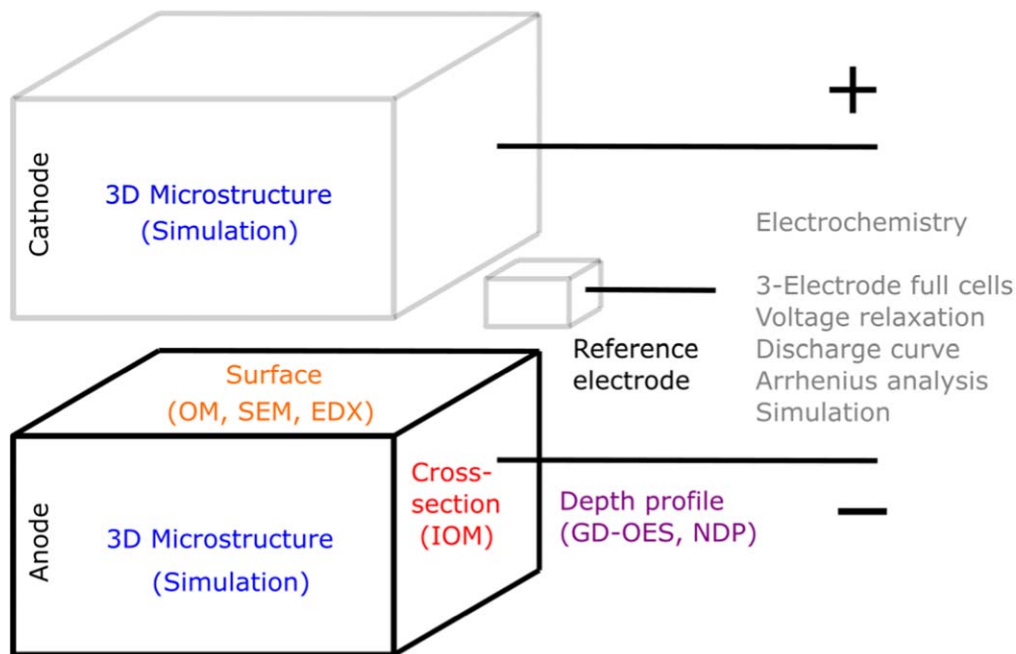


Figure 3. Overview on physico-chemical and electrochemical methods for detection of Li depositions which were considered in this review.

profiling (GD-OES, NDP), as well as electrochemical (3-electrode full cells, voltage relaxation, discharge voltage curves, Arrhenius analysis) techniques. The available simulations cannot be assigned to just one of these categories, since they include 3D resolved microstructures of anodes and cathodes (including their surfaces) and they connect the physico-chemical to the electrochemical methods.

GD-OES is a spectroscopic method that provides depth-resolved information about the elemental distribution and in a sample from the anode surface to the current collector.^{12,16–18,35,36,47,76,78,131,160–166} An Ar plasma is used to remove sample atoms layer by layer in a sputtering process. The ejected atoms undergo further collisions with the plasma components, getting excited and emitting photons of characteristic wavelengths upon energy release.¹⁶⁷ In the spectrometer unit, the emitted light is split into its spectral components and their intensities are detected by photomultiplier tubes or a charge-coupled device (CCD).¹⁶¹ After calibration with a set of lab-coated reference samples of known Li content, the amount of Li in anodes from disassembled Li-ion cells can be quantified.³⁶ Using semi-quantitative approaches, it is possible to determine the minimum amount of metallic Li in the sample and thus detect Li deposition on graphite^{36,47} and graphite/Si.^{18,35,113}

NDP is a non-destructive nuclear analytical method that is highly sensitive to some specific light isotopes (e.g. ^3He , ^6Li , ^{10}B , ^{14}N , ...) ^{168,169} and is used to obtain depth specific content of these elements in solids. Upon irradiation of a material with a neutron beam, these isotopes absorb the neutrons and emit charged particles with well-defined energies. E.g. absorption of a neutron by ^6Li isotope results in creation of triton (^3H) and alpha (^4He) particles. Energy loss of these charged particles is measured after they penetrate to the surface. The amount of energy that the alpha and triton particles lost in this process is directly related to the original position of the neutron absorption in the material. The energy loss depends on their path length, material composition, and material density. In the case of battery electrode characterization, a depth profile of ^6Li content within the sample can be determined.^{170,171} NDP has therefore become a widely used characterization technique, which provides information about the Li content originating from all Li containing compounds in the analysed electrodes.^{172–176}

In situ optical microscopy (IOM) methods have been used to investigate Li deposition on Li metal anodes^{143,144,177} and other anode

materials.^{68,72,142,178–180} By choosing a cross-sectioned full cell optical setup, a near realistic cell configuration was reached by Hogrefe et al.^{68,178,181} Due to the cross-sectional view, lithiation gradients through the anode coating can be observed by the different colours of Li-graphite intercalation compounds (Li-GICs: LiC_{18} : blue,^{180,182,183} LiC_{12} : red,^{180,182,183} and LiC_6 : yellow/golden^{180,182}).^{68,178} Additionally, the nucleation of Li depositions, growths of Li dendrites, and internal short circuits by these dendrites can be directly observed, which become evident by the appearance of shiny-silver, dendritic, and moss-like structures on the anode.⁶⁸

Ex situ OM is based on the reflectance of visible light from the sample surface. The resolution of OM is physically limited by Abbe's diffraction limit, first described in 1873,¹⁸⁴ which is $\sim 0.2 \mu\text{m}$.^{185,186} With OM, Li depositions can be identified as shiny-silver deposits with their dendritic and moss-like structures on the anode surface differing strongly from the graphite particles and the pores in between. As OM also provides color information from the sample, the Li amount of Li in a graphite particle and the spatial homogeneity of the local SOC of an electrode can be assessed.^{68,117,178,180} In contrast to IOM described above, the use of ex situ OM is not as widespread in the literature. The advantage of OM is that, when placed inside a glovebox, the electrode surface can be viewed directly by optical microscopy without a glass window protecting the lens from reactive active materials and the electrolyte, allowing images with a higher resolution and low preparation effort.

SEM utilizes a focussed electron beam that is scanned over a small area of the specimen to acquire a 2D image with high resolution. The interaction of the primary electron beam with the sample creates different types of electrons, which carry specific information from the sample, such as sample topography (secondary electrons) or composition (backscattered electrons), and which are used to generate the image.¹⁸⁷ In addition, the electron beam creates characteristic X-rays, which can be used for chemical analysis by means of EDX.¹⁸⁸ Li depositions can be identified by their morphological characteristics, as their dendritic, needle-like, or mossy appearance significantly differs from those of anodes without Li depositions.^{35,36,47,66,67} Due to the small area measured by SEM, it is important to observe several spots of the sample to get a reliable picture on the presence of Li depositions. Detecting Li with EDX is challenging as X-rays generated by the interaction of the electron beam with Li cannot be detected by most common systems. For the

detection of Li with EDX, a windowless detector with high sensitivity and high energy resolution in the low eV range is necessary.^{150–152,189} However, direct detection of Li deposition by EDX was not validated yet and is therefore not explicitly included in the WF.

In 3-electrode full cells, the anode potential becomes measurable. Deposition of bulk Li metal is thermodynamically possible when the anode potential drops below 0 V vs Li/Li⁺.^{8,34,40,105} Kinetic effects might shift the onset half-cell voltage for Li plating by a few tenths of millivolts.¹⁹⁰ Still, the “0 V criterion” serves as a tractable condition to exclude Li deposition on the anode surface. In order to monitor the anode potential, the insertion of a third electrode, mostly Li metal reference electrodes, allows to test the experimental conditions (e.g. temperature, current) when 0 V vs Li/Li⁺ is reached.^{34,40,191}

Simulation of Li deposition in Li-ion batteries is an established method to assist, guide, or complement experimental techniques. The reduction of Li⁺ ions to Li metal occurring at the particle surface of active materials is modelled based on Butler-Volmer-like kinetics. In this model setup Li deposition on the solid competes with Li intercalation into the solid. A mass balance of the plated Li is used to calculate the temporal evolution of the Li film on the particle surface. Arora et al. were the first to report a continuum model for Li deposition in Li-ion batteries.¹⁰¹ The model was adopted and also extended in several studies,^{88,91,92,97,100,102,107,192–194} e.g. by including thermal effects,^{91,97,102} additional active materials,^{97,193} or the formation of dendritic structures.^{106,194} Moreover, both irreversible and reversible Li deposition was investigated in simulation studies.^{100,106,193} In the latter case Li stripping was considered either by chemical intercalation into the active material or dissolution in the electrolyte.^{88,89,97,100,102,106,107,193} O’Kane et al. pointed out the importance of the correlation of degradation mechanisms.¹⁹² While typically the effect of the SEI on Li deposition was neglected, recent publications suggest varying modelling strategies to describe interactions of these two degradation phenomena.^{89,91,97,98,106,193,194} Due to high computational complexity, several simulation studies determine the risk for Li deposition by merely calculating the overpotential of the deposition reaction.^{96,102–104,107} Please note, that in contrast to experimental 3-electrode measurements (see above) the Li overpotential, or “0 V criterion,” is evaluated locally at the electrode/electrolyte interface in simulations.

Tracking of the cell voltage in the relaxation phase after charging can give a hint on reversible Li depositions.^{18,56,62,72} The mixed potential of lithiated graphite in contact with re-intercalating Li metal leads to a different shape of the voltage relaxation curve.^{18,56,62,72} In particular, the derivation of the voltage relaxation curve with respect to time also shows a minimum in the case of Li depositions.⁵⁶ The position of the minimum is an indicator for the amount of deposited/re-intercalated Li.⁵⁶

Monitoring the cell voltage during a (slow) discharge can give a hint on reversible Li depositions.^{46,47,52,61} In case stripping of previously deposited Li is happening during the discharge, a plateau is observed at the beginning of the discharge due to the mixed potential of lithiated graphite and Li metal.^{46,47,52,61} We note that both, the voltage relaxation and the discharge curve should be compared with a fresh cell without Li deposition as a baseline.

Aging rates can be obtained from capacity fade as a function of time or cycles.^{11,37,38,45,50,195} The aging rates are temperature dependent and often follow an Arrhenius-like behavior.^{11,37–39,45,50,195} While the values of the activation energies obtained from such Arrhenius plots must not be over-interpreted, negative apparent activation energies (faster aging with lower temperatures) indicate Li plating.^{11,37,38,45,50,195}

In case of anode samples with Li depositions, we recently compared GD-OES depth profiling with SEM, voltage relaxation,³⁵ and OM,³⁵ as well as NDP.¹¹³ Li plating was consistently indicated by voltage relaxation curves^{46,47} and capacity increase during rest times^{46,47} (both indicating Li re-intercalation into graphite), a voltage plateau at the beginning of the discharge curve^{46,47} (indicating Li stripping), low Coulomb efficiency^{46,47}

(indicating side reactions), faster aging at lower cycling temperatures^{46,47} (positive slope in Arrhenius plot of aging rates indicating Li plating), as well as GD-OES depth profiling^{36,46,47} and dendritic structures in SEM measurements.^{36,47} Anode potentials vs Li/Li⁺ from 3-electrode measurements in full cells at ZSW were correlated with aging rates obtained at other institutes and showed consistent results.³⁴ The consistency of Li deposition occurring mainly on the surface of anodes is consistently shown for GD-OES, NDP, IOM, and simulations in WF 2 of this paper.

Workflows for Detection of Li Depositions

In this section we present different WFs for the analysis of Li deposition with a focus on experimental methods. The WFs answer the question if, where, and under which conditions Li deposition occurs in aged Li-ion cells. Simulation approaches (digital twins) complement the experimental techniques and support the analysis. Additional characterization of pristine cells is required to parameterize and validate the digital twins of the cells. However, predictive capabilities of simulation approaches are highly relevant to analyze critical geometrical scenarios on cell and electrode level (WF2), as well as optimal operation conditions (WF3).

WF 1: Is Li deposition present in an aged cell?—In some cases, it might be required to know if Li depositions are present in an aged cell. For example, if cells are intended to be re-used in second life applications, Li depositions should be excluded because they could have negative effects on safety^{8,40,46–51} and could even accelerate the following aging.¹⁹⁵

If the cells originate from lab-tests, the maximum rest time between the end of cycling and cell disassembly of two hours should be complied with (see discussion above). However, cells in this WF may also originate from applications in the field where they have been used under real-life conditions. One difference to cells tested in the lab is that cells used in the field are usually not continuously charged and discharged. Instead, cells in applications are rather only partly charged/discharged, and may have extended rest times. Furthermore, in case of cells from applications, it is often not possible to comply with the maximum rest time of two hours. In consequence, if Li depositions are detected in cells from the field, they correspond mostly to irreversibly deposited Li and part of them have most likely reacted with electrolyte.

Figure 4 shows a WF for determining if Li depositions are present in an aged cell. First, the cell is pre-inspected, which includes the measurement of internal resistance and cell mass, as well as capacity determination. Comparison of the measured cell mass with that of a fresh cell of the same type gives a hint on possible leakage of the cell. In case of leakage, H₂O and O₂ are very likely present in the cell and will react with Li and change the results of the analysis. If available, aging data might be evaluated as well, e.g. regarding voltage relaxation after charging,^{47,56,62,72} or features in the discharge curve,^{46,47,52,61} faster aging during lower temperatures compared to aging at higher temperatures,^{11,37,38,45,47,50} or capacity recovery.^{46,53}

In order to reduce the electrochemical energy content of the cell and therefore the risk for the experimenter, the cells should be discharged to the end-of-discharge voltage before disassembly. Discharge below the end-of-discharge voltage can result in Cu dissolution from the anode current collecting foil.^{163,164,199–203} Cu dissolution to Cu²⁺ or Cu⁺ gets thermodynamically allowed when the anode potential increases above 3.38 V or 3.56 V vs Li/Li⁺, respectively.¹⁶⁴ Furthermore, Flügel et al. showed for seven types of commercial cells, that the additional discharge from the end-of-discharge voltage to 0 V leads only to minor decreases of cell energy corresponding to negative SOCs of –3% to –9%.¹⁶⁴ Therefore, the end-of-discharge voltage given in the data sheet is a good compromise for disassembly.⁷

It has to be considered that in discharged aged cells, a part of the Li might have been stripped or electrically disconnected. Therefore,

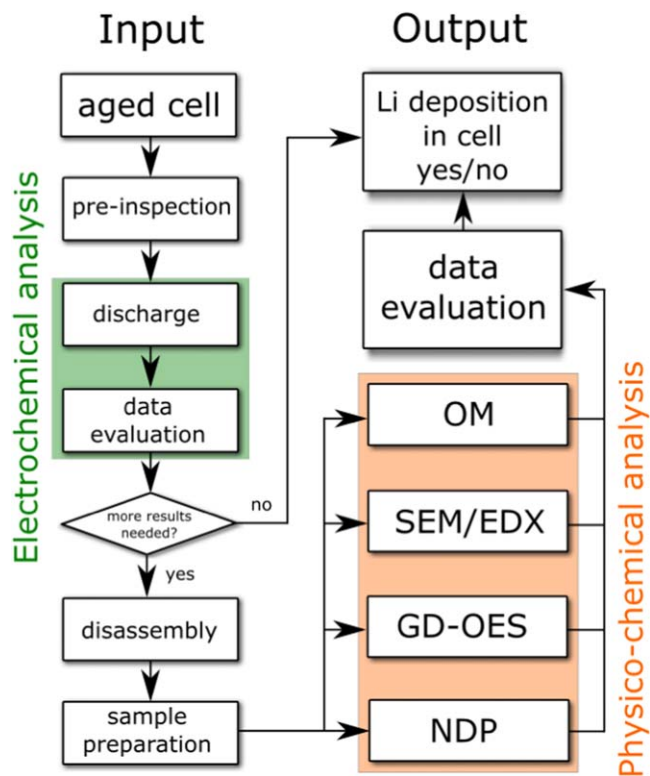


Figure 4. WF 1 for answering the question if Li deposition is present in an aged cell (OM = optical microscopy, SEM/EDX = scanning electron microscopy/energy dispersive X-ray spectroscopy, GD-OES = glow discharge optical emission spectroscopy, NDP = neutron depth profiling).

the detected Li depositions on the anode from a discharged aged cell by physico-chemical methods is the sum of irreversible and “dead Li.”

The discharge curve may yield first hints on Li deposition.^{46,47,52,61} Fig. 5 shows a shoulder in the discharge curve of a cell with Li plating.⁴⁶ This shoulder results from Li stripping as a parallel reaction of Li de-intercalation from the anode.⁶¹ However, care must be taken in the interpretation of this shoulder, since other effects might also affect the voltage curve:

(1) The cell temperature influences the cell voltage^{204,205} and therefore might influence the discharge voltage curve as well. Hence, it is imperative to monitor the cell temperature while discharging, for instance, via a thermocouple that is fastened to the surface of the cell.

(2) The electrochemical data obtained from a cell reflects the entire anode and cathode region. If Li depositions are only present in a limited section of the anode, the plateau may not be significant in the discharge curve.

(3) Only reversibly deposited Li can be stripped during discharge. Electrically disconnected Li (“dead Li”) or Li metal covered by a thick passivation layer will not contribute to the plateau in the discharge voltage curve.

Hence, the plateau observed in the discharge voltage curve may merely indicate the existence of reversible Li depositions in a cell. Nonetheless, the lack of a voltage plateau does not necessarily preclude the existence of Li depositions, for instance, if Li depositions are present in limited regions of the anode only or in case of “dead Li.” Since electrochemical measurements are averaging on the whole anode area in the cell, small amounts of deposited Li might not lead to features in the voltage curves.

We would like to note that particularly the quantification of irreversible and even reversible depositions is not possible from

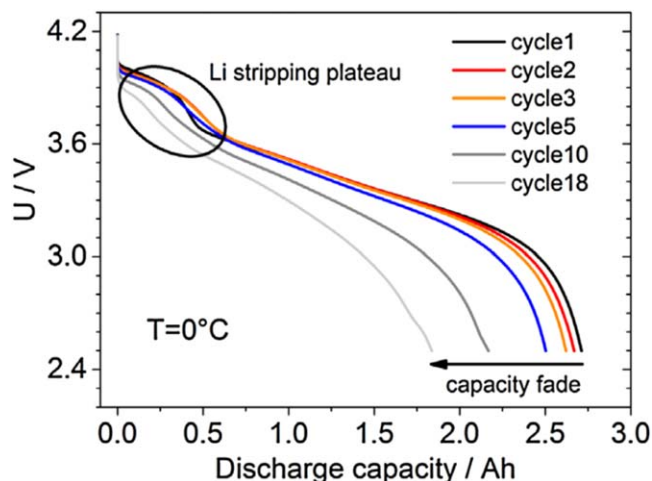


Figure 5. Voltage plateau in discharge curves as an electrochemical indicator for reversible Li deposition on anodes by Li stripping. Reprinted with permission from Ref. 46.

discharge voltage curves. For quantification of the amount of deposited Li, more sophisticated physico-chemical experimental methods are needed as discussed below.

If the shoulder in the discharge voltage plateau is already observed in an early stage of the WF, it has to be decided whether this information is enough to judge if the cell contains Li depositions or if further methods have to be applied. In case the voltage plateau is not observed, further measurements are required (see yes/no decision in Fig. 4).

Further measurements within WF 1 necessitate cell disassembly. To ensure a well-controlled environment, the disassembly should be performed inside an Ar-filled glovebox to prevent reactions of H₂O, O₂, and N₂ with the deposited metallic Li in the cell.

During cell disassembly, the separation of anode, cathode, and the separator must be carried out with care by a trained expert. Stacked cells (pouch and prismatic cells) contain several anodes, cathodes, and separators, while wound jellyrolls (cylindrical, pouch, and prismatic cells) contain only one rolled anode and cathode. The specimens for subsequent examination should be collected from the most prominent regions, e.g. white or grey deposits (see Figs. 8a–8c as examples).

As an example, Fig. 6 shows consistent measurements of complementary methods for graphite/Si anodes with and without Li depositions.³⁵ Figures 6a, 6b displays SEM measurements without (0.5 C charging) and with Li dendrites (1 C charging), respectively.³⁵ Figures 6c–6e show OM measurements in a glovebox, where the amount of dendritic structures is increasing with SOC.³⁵ GD-OES measurements of samples without Li depositions (0.5 C, black data) and with Li depositions (1 C, red data) are depicted in Fig. 6f.³⁵

The ex situ methods OM³⁵ and SEM^{35,36,47,66,67} are comparably cheap and fast and deliver further hints on Li depositions, due to their dendritic growth (see Figs. 6a–6e). It is noted that the dendrites are still visible, even if the samples had air contact before SEM measurements. Figure 7 shows the surface of a graphite anode at 80% SOC, partially covered by Li. When exposed to air, the lithiated graphite particles and the Li deposition change optically with increasing exposure time. The color change of the graphite particles is known to be caused by spontaneous de-lithiation in the presence of air/humidity, and the formation of Li-(hydro)oxides on the surface of the graphite particles.²⁰⁶ The de-lithiation proceeds through sequential stages—from LiC₆ (gold) to LiC₁₂ (red), LiC₁₈ (blue), and finally graphite (black/gray). After only 30 s of air exposure, almost all of the previously golden and red graphite particles have turned blue. After 60 s, most particles have turned blue or black. After 300 s on air, all graphite particles are black and further air exposure does not lead to any further clear optical change.

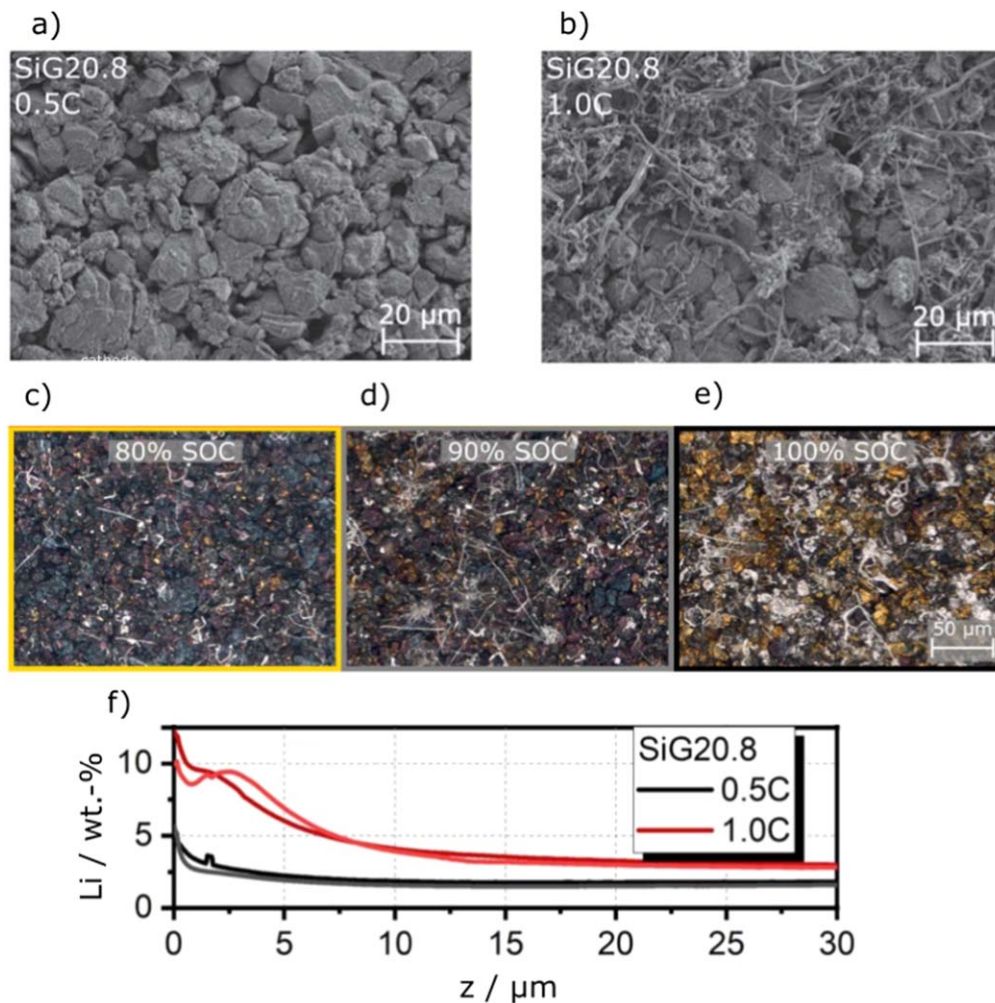


Figure 6. Ex situ measurements of graphite/Si anodes with 20.8 wt% Si in Post-Mortem analysis. (a), (b) SEM measurements of graphite/Si anode a) without Li depositions (after charging at 0.5 C) and (b) with Li depositions (after charging at 1 C). The samples in (a), (b) were transported through air from an Ar-filled glovebox to the SEM device. (c)–(e) ex situ OM images of graphite/Si electrodes from half cells opened at different SOC. The samples in (c)–(e) were investigated without air contact inside an Ar-filled glovebox. (f) GD-OES measurements of anode samples without (black curves, after 0.5 C charging) and with Li depositions (red curves, after 1 C charging). The two red and black curves are reproduced GD-OES measurements. The GD-OES measurements were conducted after air contact. Reprinted with permission from Ref. 35.

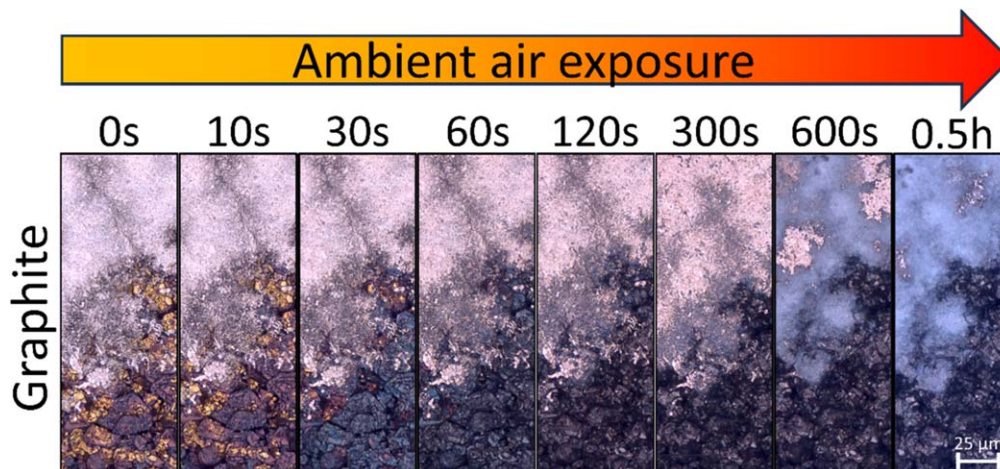


Figure 7. Ex-situ OM images of a graphite electrode after charging to 80% SOC at a rate of 1 C showing changes of the visual appearance of deposited Li (grey/silver) and inhomogeneously lithated graphite (gold and blue/purple) after exposing the sample to ambient air.

With Li depositions, the optical changes occur later, starting with a matt haze after about 300 s (see Fig. 7). With increasing exposure to air, this haze turns blueish (600 s) and makes it hard to recognize the fine structures of the Li depositions by *ex-situ* OM. The main reaction products of Li with moist air are most likely Li oxides and hydroxides.

Observation of dendritic structures on an anode by SEM or OM is a hint on the presence of Li depositions. However, these methods do not give evidence on Li depositions since Li is not chemically proven and e.g. Cu grows also in a dendritic manner.^{202,207,208} However, Cu and Li dendrites might be differentiated by their color in OM and by image contrast in SEM measurements. On the contrary, the lack of dendritic structures observed via SEM does not definitively prove the absence of Li depositions. For microscopy measurements, it is generally necessary to consider that the observed area is relatively small. Therefore, in a WF it is necessary to measure several positions of the samples to ensure an accurate representation.

GD-OES and NDP are complementary depth profiling methods which were validated against each other.¹¹³ Figure 6f shows GD-OES measurements of a graphite/Si anode without (black curves) and with Li plating (red curves).³⁵ The Li content on the anode surface is significantly increased in case of Li depositions. The Li amount detected by GD-OES corresponds to the sum of Li being intercalated in the anode, SEI growth and Li deposition. In order to keep the amount of intercalated Li as low as possible, it is necessary to investigate anodes from cells disassembled in the discharged state.

To determine the contribution of metallic (deposited) Li by GD-OES, a semi-quantitative approach has been developed by Ghanbari et al. for graphite anodes assuming that Li_2O is the only SEI component and that all oxygen (O) detected originates from this species.³⁶ Therefore, it is possible to calculate the demand of the required Li in Li_2O to match with the measured O content. As Li_2O is the SEI compound binding the highest Li amount, this method gives the maximum proportion of SEI growth and the minimum proportion of metallic Li on the total Li content in the anode.³⁶ If the difference between the detected Li content and the calculated Li amount in Li_2O is positive, Li was deposited on the graphite anode surface.³⁶

In case of graphite/Si anodes, Li silicates as well could be assumed to be the predominant SEI component forming on Si components.¹⁶ However, due to the presence of formed SiO_x species in this kind of anodes, the amount of O detected by GD-OES can no longer be traced back to Li_2O only.¹⁸ Therefore, an enhanced GD-OES method was developed by Flügel et al. for Li deposition on graphite/Si anodes.¹⁸ In order to determine the O content originating from the Li_2O species (which is used analogously to calculate the required amount of Li to form Li_2O), the measured O content is corrected by the amount of O bound in SiO_x using the amount of Si detected by GD-OES (see Eq. 3 in Flügel et al.¹⁸). Since the exact stoichiometry of the SiO_x component is unknown, this approach results to a corridor within which the minimum amount of deposited Li on graphite/Si anodes is located.¹⁸

Once all experiments have been completed, the data should be analyzed comparing the results of the different electrochemical and physico-chemical analysis methods to decide if Li depositions are present in the investigated cell or not. It is noted, that in some cases it might not be necessary to apply all proposed characterization methods. However, the combination of the proposed complementary methods produces more reliable results. We further note that the analysis methods do not necessarily have to be performed in parallel, but alternatively in series (see Fig. 1 and discussion above).

WF 2: Where in a cell do lithium depositions occur?—Figure 8 shows different morphologies of Li depositions on anodes.^{36,54,209} An example of an anode with Li plating—the deposition morphology which is most homogeneous on a macroscopic scale—is shown in Fig. 8a.⁵⁴ It is noted that although Li plating looks homogeneous on a macroscopic scale, its microstructure is still dendritic.^{36,47} Homogeneous Li plating occurs mainly during charging at low temperatures.^{33,47,52,54}

Different groups^{70,84,209,210} observed marginal Li depositions, i.e. local deposition at the border of an anode. An example of marginal Li deposition on anodes of a 22 Ah pouch cell is shown in Fig. 8b.²⁰⁹ Grimsman et al. explain marginal Li depositions by an imbalance of the Li distribution in the cathode forming by Li diffusion into the anode overhang after charging.²⁰⁹ Additionally, Tang et al. found in simulations that the current density can be significantly increased at the edge of the electrodes.⁹⁵ Other reasons for marginal Li deposition could be lower temperatures at the edges of the cell, misalignment of the electrodes during manufacturing, a too small anode overhang, or a different coating thickness at the edge of the anode.⁸ Unlike Li plating, marginal Li deposition does not necessarily occur at low temperatures only.²⁰⁹

Local Li depositions occur preferentially at high temperatures (above $\sim 45^\circ\text{C}$) in combination with high charging currents,^{33,36,78,80,130,211} or due to pressure inhomogeneities.⁴² An example of local Li deposition is shown in Fig. 8c.³⁶ A mirror-like pattern from the depositions on the anode was found on the separator and the cathode by different authors.^{78,80} Reasons for local Li depositions can be locally high charging currents at the border of dried areas or gas bubbles^{36,80,130} or at defects of the separator with closed pores.²¹¹ Foreign particles²¹² which are weakening the separator, could possibly also lead to locally increased current densities and therefore to local Li deposition. Additionally, local inhomogeneities of the coating thickness of anode or cathode, as for instance observed by Wu et al.,²¹² will lead to a locally different N/P ratio and therefore also to the risk of local Li deposition.

Additionally to the distribution of Li depositions on anodes, the morphologies and the amounts of deposited Li might differ throughout the different anodes in an electrode stack inside a cell and for the different coating sides of the anodes. Therefore, all anodes from an electrode stack (e.g. from a pouch cell or a prismatic cell) should be investigated carefully (Fig. 8e).

The unrolled jellyroll of a cylindrical cell is depicted in Fig. 8f. Cylindrical cells typically contain only one anode in the jellyroll. In similarity to the case of stacked electrodes, the positions in an unwound jellyroll can be defined by introducing x/y axes to the anode. In case of cylindrical cells, it is important to mark the inner and outer parts of the jellyroll, corresponding to the positions near to the core and to the housing of the cells, respectively. Furthermore, it is important to mark the concave and convex side of the electrodes, as e.g. differences in the porosity and aging might occur.²¹³ Flat wound jellyrolls can be present in pouch and prismatic cells alternatively to stacked electrodes. Special attention should be paid to comparing the flat and curved parts of the electrodes, since differences can be expected in the regions with high curvature.^{213–216}

Figure 8d depicts a cross-section of an anode. Inhomogeneities in anodes from aged cells can also occur in the anode coating. Therefore, the z-axis marks the path into the anode depth, from the anode surface ($z = 0$, near the separator) to the current collector. We note that in case of Li plating on the surface of the anode coating, the surface ($z = 0$) is shifted to the surface of the plated Li.

WF 2 for answering the question of where in/on the anodes Li deposition occurs in a cell is shown in Fig. 9. An aged cell is pre-inspected, discharged, and disassembled, similarly as in the WF 1 (see previous section). The electrochemical data from aging and from the discharge curve might give hints on the presence of Li depositions in the cell, however, not where it is located in the cell.

The samples are taken from areas with suspicious features that could possibly be Li depositions. For this, all anodes and all their coating sides must be carefully examined. The positions on an anode should be marked using the x/y coordinates given in Figs. 8a–8c, 8e for pouch cells and in Fig. 8f for cylindrical cells (e.g. 18650, 21700, 46800). After performing OM, SEM, GD-OES, and NDP with these samples, it can be judged if the suspicious features at the selected x/y positions contain Li depositions from experimental point of view.

Additional to the analysis of an aged cell, structural and electrochemical measurements on fresh cells allow the determination

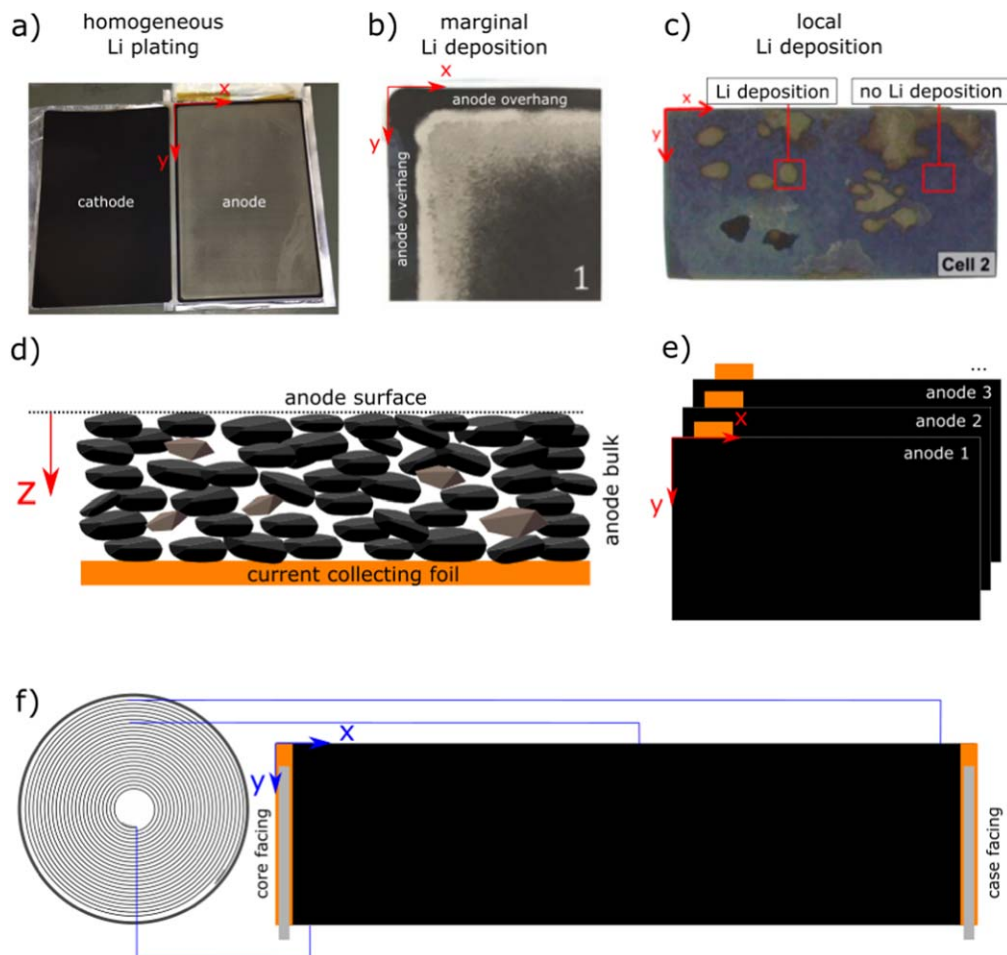


Figure 8. (a)–(c) Different morphologies of Li depositions on anodes from aged pouch cells with different graphite/NMC chemistries. (a) Homogeneous Li plating on an anode of a 20 Ah pouch cell after 8 cycles at 0.5 C and 3 cycles at 0.6 C at -5°C .⁵⁴ (b) Marginal Li deposition on the corner of an anode of a 22 Ah pouch cell after 4 full cycles with 2.5 C charging rate and a cut-off voltage of 4.15 V at 25°C .²⁰⁹ (c) Local Li deposition on the anode of a 16 Ah pouch cell after cycling at 45°C with 3 C charging until 89.4% capacity retention.³⁶ Definition of x/y-plane for anodes from pouch cells (a)–(c), (e) and for an unrolled anode from a cylindrical cell (f). (d) Definition of z-direction in the anode coating. In case of Li plating on the surface of the anode coating, the surface ($z = 0$) starts on the surface of the plated Li. The schemes in (d)–(f) are not drawn to scale. (a), (b) Reprinted with permission from Elsevier,^{54,209} Copyright Elsevier. (c) Reprinted with permission.³⁶ Copyright American Chemical Society.

of input parameters for simulations and validation of the digital twins.^{89,91,96,97,106} Specific care has to be taken to balance high spatial resolution and sample volume during imaging and reconstruction of representative electrode microstructures.²¹⁷ Both parameters significantly affect the determination of characteristic microstructural properties of cell level simulations like tortuosity and specific surface area. The deposition of metallic Li within the cell induced for example by tab tearing⁹⁶ or non-uniform temperature distributions⁹¹ were simulated and analyzed. At this scale are not only electrochemical models but also equivalent circuit models and data-driven models utilized.¹⁹³

A modified version of WF 2 can also be applied to answer the question where in the anode coating of a given area Li depositions occur (z-direction in Fig. 8d). In this modified WF, IOM is added. Theoretically, Li could (i) deposit homogeneously through the depth of the anode, (ii) it could be randomly distributed, or (iii) enriched on the anode surface (near the separator). The depth profiling methods GD-OES^{18,35,36,47,76,78,113} and NDP^{113,196} provide Li depth profiles several μm from the surface. However, both methods cannot distinguish between metallic, oxidized, or intercalated Li. Therefore, the cells should be disassembled in the discharged state to avoid the presence of larger amounts of intercalated Li. Simulations on electrode level, ideally microstructurally resolved simulations on reconstructions of the electrodes, provide information on Li dynamics with high spatial resolution. The simulations allow to

deconvolute local information on intercalated Li, metallic Li,⁸⁸ and SEI thickness.²¹⁸ Thereby, the simulations can be correlated to results of depth profiling methods and provide additional insight on the influence of local inhomogeneities^{88,219} on metallic Li deposition.

In contrast, OM and SEM measurements of the anode surface are not able to determine the distribution of deposited Li in the anode coating. Both methods cannot make any statements on the Li distribution in the z-direction apart from the surface ($z = 0$ μm). For instance, Figs. 6b–6e show that Li dendrites are present on the anode surface, however, the data do not contain information on deeper layers of the anode coating.

For different cell types, GD-OES, NDP (Fig. 10a),¹¹³ IOM (Fig. 10b),⁶⁸ 3D microstructurally resolved simulations (Fig. 10c),^{87,88} as well as OM,³⁵ SEM on the anode surface³⁵ lead to the consistent result that Li depositions occur mainly on the anode surface, i.e. near the separator. A consistent result was found for GD-OES depth profiling of samples from different types of commercial and pilot-line built Li-ion cells with Li depositions.^{18,35,36,47,76,78} For graphite anode samples from the same type of 16 Ah pouch cells consistent results were obtained for GD-OES,³⁶ SEM of cross-sectioned anodes,³⁶ EDX mapping of the oxygen content of GD-OES craters,³⁶ and ^7Li NMR.⁸⁰

Simulations showed that the criterion for Li deposition is fulfilled first on the anode surface.^{59,86,89,101,102} In consistence, IOM

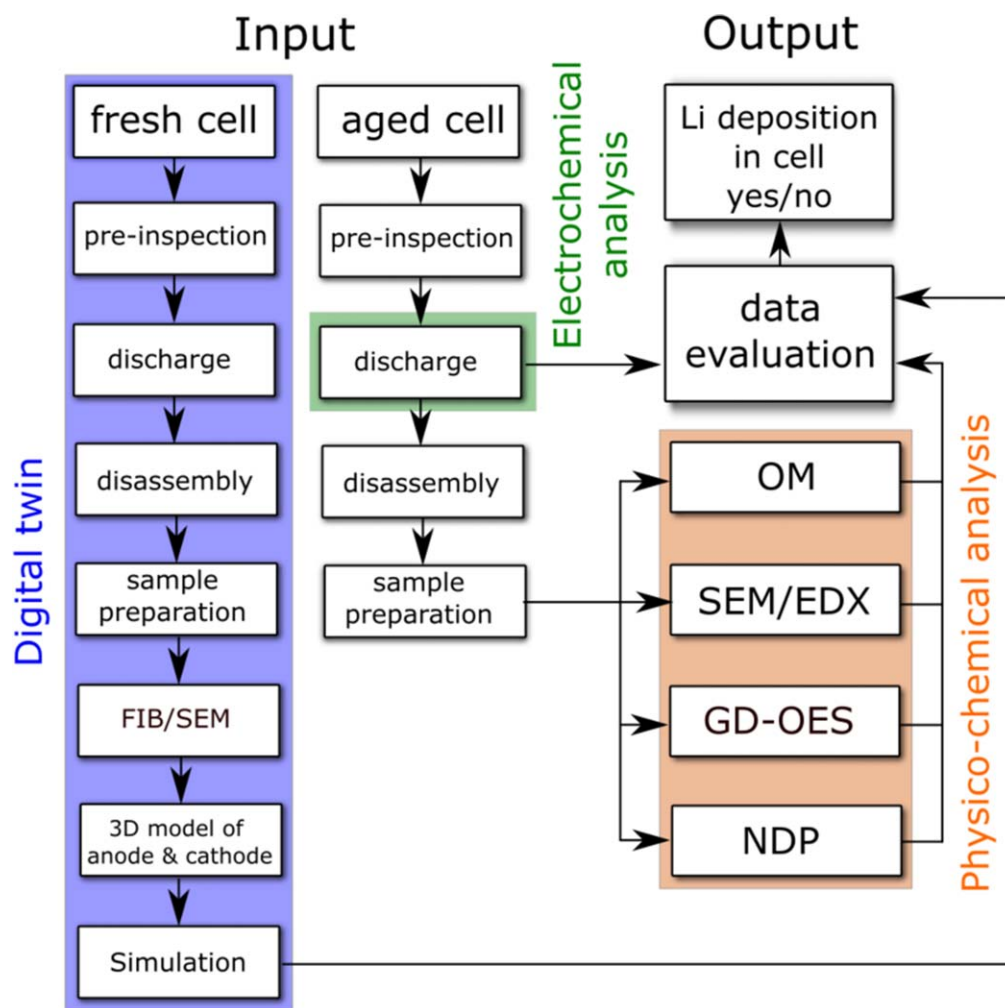


Figure 9. WF 2 for answering the question where in a cell do Li depositions occur (FIB/SEM = focused ion beam milling with scanning electron microscopy, OM = optical microscopy, SEM/EDX = scanning electron microscopy/energy dispersive X-ray spectroscopy, GD-OES = glow discharge optical emission spectroscopy, NDP = neutron depth profiling).

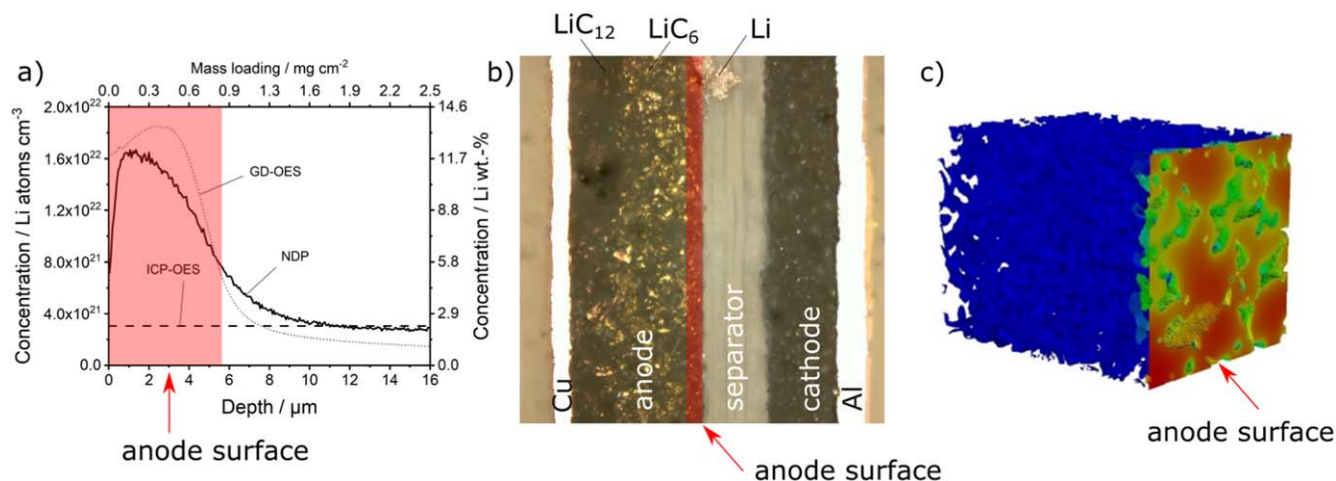


Figure 10. Determination of Li depositions in the depth of anodes (z-direction). (a) GD-OES and NDP depth profiling (graphite/Si anodes from a commercial cell), (b) IOM image of cross-sectioned full cells (graphite anodes), and (c) heat map indicating Li depositions of different thickness at the end of a 3D charge simulation (3D structure from anode of the same commercial cell as in (a)). Color scale from blue (no Li deposition) to red (maximum Li deposition thickness). (a) Modified with permission from Ref., 113 (b) modified with permission from Ref. 68.

measurements showed by the color change of lithiated graphite that the anode surface gets lithiated first for increased charging C-rates. The higher diffusion barrier for Li in higher lithiated graphite^{220,221}

(e.g. 0.308 eV for $\text{Li}_{0.2}\text{C}_6$ vs 0.4 eV for LiC_6)²²⁰ and higher lithiation of the particle surfaces²²² contributes to favoring Li depositions on the anode surface instead of only intercalation into graphite.

WF 3: Under which operating conditions does Li deposition occur?.—Increasing the cycle life is possible by avoiding Li depositions during charging.^{8,10,11,34,35,37,38,40,223,224} Li depositions can be avoided by keeping the anode potential positive vs Li/Li^+ .^{8,10,34,40,45,57,86,162,181,225–227} One difficulty is that many cell types (e.g. all commercial cells) do not contain a reference electrode, so that the anode potential cannot be measured. In the laboratory, however, it is possible to construct 3-electrode full cells that include a reference electrode.^{34,45}

One approach to increase the cycle life of commercial 2-electrode cells by avoiding Li depositions is to implement reference electrodes in 3-electrode prototype cells and use the results of the anode potential measurements later in 2-electrode cells without reference electrode.¹⁸¹ Alternatively, electrodes from commercial 2-electrode cells can be reconstructed into 3-electrode full cells to measure anode potentials.^{34,40,45} Although such approaches do not take aging into account, cycle-life was shown to increase significantly in the corresponding 2-electrode cells.^{34,40,45} Additionally, charging protocols based on simulation predictions have been successfully developed.⁹⁷

We would like to point out that it is very important to determine the anode potential vs Li/Li^+ in full cells, e.g. including a graphite/Si anode, a NMC811 cathode, and a Li reference electrode. The anode/cathode interaction is a crucial aspect of full cells. As only the difference between cathode and anode is measured in 2-electrode cells, overvoltages on anode or cathode side can shift the potential of the other electrode in an undesired direction leading to harmful side-reactions.^{10,228,229} Consumption of active Li^+ can also cause undesirable shifts in the electrode potentials.²³⁰ By monitoring the individual electrode potentials, the identification of the aging mechanism of cells can be supported.^{34,200,231}

Figure 11 shows a WF for determining the operating conditions to avoid Li depositions. This procedure is possible for both, commercial cells and prototype cells. In case of prototype cells, where the electrodes, electrolyte, and separator are typically available before they are built into a cell, they can be used directly for further analysis. Also in case of building 3-electrode full cells with reference electrode, the electrodes, electrolyte, and separator can directly be used to build these cells. Detailed structural and electrochemical characterization on each component provides information and input for creation of digital twins. Additionally, data-driven techniques can be used to inform and enhance the models.^{193,232}

In case of commercial cells (as shown in Fig. 11), the effort is higher, since cell disassembly is needed to obtain the material composition in the cells. Special care must be taken to avoid contamination of the electrodes (active material anode/cathode, humidity, oxygen) during disassembly. Consequently, disassembly must be carried out in an Ar-filled glovebox, while after washing removal of electrode coatings from the back of electrodes and cell re-assembly can be done in a dry room.^{34,40,45} One example in literature is the re-construction of graphite anodes and NMC cathodes from commercial 16 Ah pouch cells into 3-electrode pouch cells with a Li reference electrode.³⁴ The experiments showed a high reproducibility of the anode potential measured at various temperatures, ranging from 5 °C to 45 °C, for the repeated reconstruction of cells.³⁴ Furthermore, the voltage curves of the reconstructed 3-electrode cells and the original 16 Ah cells were in very good agreement.³⁴ Although, the separator and electrolyte in the reconstructed cells were not exactly the same as in the original 16 Ah cells, the aging behavior of the original cells carried out in other labs was in good agreement with the measurements of the reconstructed 3-electrode full cells.³⁴ Harvesting electrolyte from a commercial cell is generally challenging as free electrolyte is often absent. Even if the electrolyte is replicated, obtaining the exact composition remains challenging since additives may have been consumed during cell formation. On the other hand, additives are often incorporated

into the SEI, which might mostly still be present in the reconstructed cells.

The test conditions for the 3-electrode cells and the aging conditions for the original cells in Fig. 11 should be the same. Typical variations are the ambient temperature, the end-of-charge voltage (or the SOC), and the charging C-rate.^{8,11,33–35,37–39,45,50,55,56,93,94,181} For the 3-electrode cells, a few cycles are sufficient as the anode potential is measured at each charge, whereas for the aging experiments a significant amount of irreversibly deposited Li must be generated by longer cycling. The electrochemical data obtained during cyclic aging, can already give hints on whether Li depositions have occurred under the given conditions. Such hints might be obtained from voltage curves^{8,35,47,52,55,56,62,233} (see also above) and from the temperature dependency of the aging rate.^{11,37,38,45,50}

The aging rate can be obtained from the slope of the capacity fade curve.^{11,37,38,45,50} If the aging rate is increasing with lower temperatures, Li plating is likely.^{11,37–39,45,50,195} This behavior is typically determined from an Arrhenius plot of the aging rates with a high temperature SEI growth branch and a low temperature Li plating branch for the dominant aging mechanism.^{11,37–39,45,50,195} In an efficient WF, it might not be necessary to measure all data for a complete Arrhenius plot, instead two selected temperatures might be sufficient to get a hint on Li deposition in the observed temperature range.

Additionally, the electrochemical data obtained during cyclic aging can be applied to train electrochemical models. Predictive power of the models allows to extrapolate aging rates and helps to avoid critical operation conditions. Hybridization with machine learning approaches or reduced models can be used to control battery operation in the battery management system (BMS).⁹⁷

The set of aging conditions might be reduced by means of a design of experiments (DoE) approach for increased efficiency.²³⁴ In software-based DoE planning, the test matrix varies several operating parameters producing experimental test plans to obtain statistically validated results with minimized effort. For example, temperature and C-rate are varied in one experiment, instead of variation of only temperature in one experiment and only the C-rate in another experiment. The more parameters are varied, the more the DoE approach can reduce the number of experiments and therefore decrease the test time and resources compared to a conventional test matrix approach.²³⁴ Additionally, data-driven techniques, such as Bayesian optimization, can help to further reduce experimental efforts.²³⁵ We note that for certain applications which run for instance at an approximately constant temperature, a reduction of the aging test plan might also be possible without DoE planning.

As part of an efficient workflow, it may be unnecessary to carry out multiple sample preparations (e.g. $n \times 4$ sample characterizations with OM, SEM/EDX, GD-OES, and NDP). Instead, the number of cells to be analyzed by analytical methods might be reduced beforehand by evaluating the data of e.g. the extreme cases.

An example of a part of WF 3 was shown by Flügler et al., who investigated Li plating on graphite and graphite/Si anodes.³⁵ The tests were conducted in pouch full cells with the same anode areal capacity for the different Si contents, i.e. the anode coating thicknesses decreased with increasing Si content.³⁵ In order to ensure the comparability of the results, the cells with different Si contents had the same N/P ratio as well as very similar electrode porosity and tortuosity.³⁵ The results of voltage relaxation curves, GD-OES, SEM, and OM showed the clear trend of a higher critical charging C-rate leading to Li plating at 0 °C with higher Si content, due to lower anode coating thickness.³⁵

The outcomes of WF 3 often result in the typical trends, i.e. a higher susceptibility to Li depositions with lower temperature, higher SOC, and higher charging C-rate.^{8,10,17,33–35,37,38,45,52–57,102} These trends can be expected for most Li-ion cell types, however, the exact parametrization needs to be measured for each cell type.

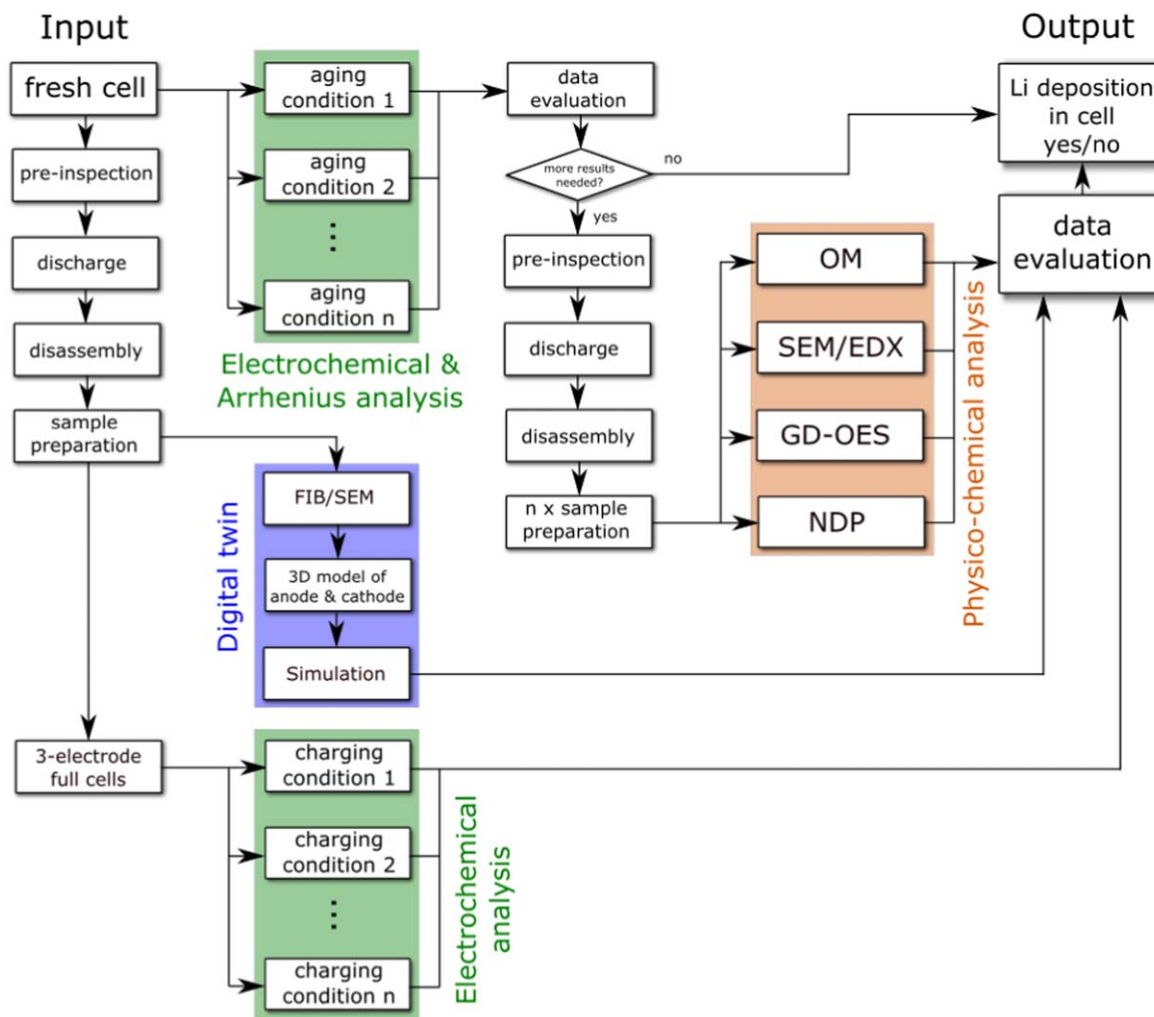


Figure 11. WF 3 for answering the question under which operating conditions Li depositions occur in a certain cell type (FIB/SEM = focused ion beam milling with scanning electron microscopy, OM = optical microscopy, SEM/EDX = scanning electron microscopy/energy dispersive X-ray spectroscopy, GD-OES = glow discharge optical emission spectroscopy, NDP = neutron depth profiling).

Conclusions

In the present paper, we reviewed literature on electrochemical and physico-chemical methods to detect Li depositions on graphite and graphite/Si anodes of Li-ion cells and developed three efficient workflows (WF 1–3) to characterize Li depositions.

The rest time between the end of a cycling test and the detection of Li depositions turned out to be critical in the WFs, since (i) Li depositions can re-intercalate into graphite and alloy with Si of the anode and (ii) deposited Li can react with electrolyte resulting in non-metallic Li compounds during rest times. We therefore strongly recommend to plan and document rest times before and during execution of a WF, respectively. Two hours maximum rest time at room temperature between the end of cycling experiments in the lab and cell disassembly can be used as a good guideline.

In terms of the characterization methods used, it is important to distinguish between methods that provide hints on Li depositions (e. g. microscopic dendritic structures on the anodes) and methods that provide an electrochemical or chemical evidence of Li metal. For the presented WFs, we choose the methods available and suitable, such as ex situ OM, SEM, EDX, GD-OES depth profiling, NDP, simulations mainly based on 3D microstructures (microstructures obtained from FIB/SEM measurements), as well as measurements of anode potentials in 3-electrode full cells with Li reference electrode, voltage relaxation and discharge curve evaluation, and Arrhenius analysis of aging rates. The methods used in the WFs were selected

since they had previously been validated against each other and had delivered consistent results.

WF 1 answers the question of whether Li deposition is present in a certain aged cell. Such cells may originate from applications where they have been used under real-life conditions in the field. Therefore, the compliance with maximum rest times is often impossible for cells from the field and the observed depositions correspond mostly to irreversible Li. Essentially, WF 1 includes inspection of the cell prior to disassembly, discharging, and analysis of the anodes. In case the electrochemical information from the discharge curves (voltage plateau as hint) is regarded to be sufficient (e.g. together with other complementary information available), it might not be necessary to disassemble the cell. However, for cells from the field this is difficult since most of the reversibly deposited Li might not be available anymore due to long rest times. Disassembly is also necessary in case Li depositions in small areas of the anode have to be excluded, since electrochemical data averages over the whole electrode area. After disassembly, OM, SEM/EDX, GD-OES, and NDP are recommended for physico-chemical analysis of the anodes.

WF 2 answers the question where Li depositions occur within a cell. Li depositions can occur (i) on different anode sheets of stacked cells, (ii) at different x/y positions on one anode of a cell, and (iii) in different z positions within the depth of an anode coating. It is good practice to compare measurements from suspicious and non-suspicious x/y positions on an anode after cell disassembly. Typical x/y distributions of deposited Li are (i) homogeneous Li plating (often after low

temperature charging), (ii) marginal Li deposition, and (iii) local Li deposition (often after charging at high C-rates and high temperatures). Regarding the distribution of Li depositions in the depth of the anode coating (z-direction), the complementary methods OM, SEM, IOM, GD-OES, NDP, and simulations revealed consistently that Li is mostly located on the anode surface, i.e. near the separator.

WF 3 answers the question of the operating conditions (temperature, charging C-rate, SOC window, ...) under which Li deposition will occur in a given cell type. 3-electrode full cells with reference electrodes are helpful to determine the onset of Li deposition via measurements of the anode potential vs Li/Li⁺ for different operating conditions. Such measurements are also possible by reconstructing the electrodes from commercial cells into 3-electrode full cells. Additionally, cyclic aging tests in combination with cell disassembly are very helpful to determine under which aging conditions Li depositions occur in a certain cell type. A software supported DoE approach can be utilized to reduce the number of experiments. The results obtained by WF 3 can give a good overview on the aging behavior of a certain cell type. WF 3 can therefore help to increase cycle life by choosing optimized operating windows. We note the results will most likely reflect the general trends (e.g. more Li plating below a threshold temperature at a given charging C-rate), however, the exact parametrization has to be measured for each cell type.

The WFs developed in this paper are very useful for avoiding Li deposition in first and second life applications, for failure analysis, and for improving battery safety and extending battery life. In addition, the bundling of highly specialized equipment together with simulation can provide a much deeper insight into the mechanisms of Li plating and thus boost the efficiency of the investigations significantly. The increased cycle life gained by the WFs has the potential to increase sustainability and reduce resource dependency on critical raw materials through longer battery use before recycling.

Acknowledgments

Funding of the project CharLiSiKo (03XP0333) in the Aqua cluster by the German Federal Ministry of Education and Research (BMBF) and project management by Projektträger Jülich (PtJ) are gratefully acknowledged. This goes along with a successful collaboration within the Aqua cluster with Adrian Lindner (KIT) from the project MiCha (03XP0317B) who performed FIB/SEM measurements and 3D reconstructions of the mentioned cells. Furthermore, the authors acknowledge the BMBF for funding the project ExZellTUM III (03XP0255) in the ExcellBattMat cluster and the German Federal Ministry for Economic Affairs and Climate Action (BMWK) for funding of the project CAESAR (03EI3046F). NDP experiments were carried out at the NPI and RC infrastructures "CANAM" and "Reactors LVR-15 and LR-0" in Řež with the support of the Ministry of Education, Youth and Sport of the Czech Republic (Projects No. LM2015056 and LM2015074). The Deutsche Forschungsgemeinschaft (DFG) is acknowledged for financial support via the International Research Training Group 2022 the Alberta/Technical University of Munich International Graduate School for Environmentally Responsible Functional Materials (ATUMS) and under Germany's Excellence Strategy EXC 2089/1 390776260 (e-conversion). The work performed at ZSW and DLR contributes to the research at CELEST (Center for Electrochemical Energy Storage Ulm-Karlsruhe).

ORCID

Thomas Waldmann <https://orcid.org/0000-0003-3761-1668>
 Christin Hogrefe <https://orcid.org/0000-0001-9952-8507>
 Marius Flügel <https://orcid.org/0000-0002-9792-0414>
 Ivana Pivarníková <https://orcid.org/0000-0002-0951-947X>
 Christian Weisenberger <https://orcid.org/0000-0001-7392-2565>
 Estefane Delz <https://orcid.org/0009-0006-8719-1760>
 Marius Bolsinger <https://orcid.org/0009-0008-9818-1095>
 Lioba Boveleth <https://orcid.org/0000-0001-9283-2397>
 Neelima Paul <https://orcid.org/0000-0002-6906-1683>
 Max Feinauer <https://orcid.org/0000-0003-2483-8257>
 Robin Schäfer <https://orcid.org/0000-0002-5204-5388>
 Katharina Bischof <https://orcid.org/0009-0004-0321-3252>

Timo Danner <https://orcid.org/0000-0003-2336-6059>
 Volker Knoblauch <https://orcid.org/0000-0001-9075-9085>
 Peter Müller-Buschbaum <https://orcid.org/0000-0002-9566-6088>
 Ralph Gilles <https://orcid.org/0000-0003-2703-4369>
 Arnulf Latz <https://orcid.org/0000-0003-1449-8172>
 Markus Hölzle <https://orcid.org/0009-0004-8278-1089>
 Margret Wohlfahrt-Mehrens <https://orcid.org/0000-0002-5118-5215>

References

1. M. Broussely, S. Herreyre, P. Biensan, P. Kasztejna, K. Nechev, and R. J. Staniewicz, *J. Power Sources*, **97–98**, 13 (2001).
2. M. Broussely, P. Biensan, F. Bonhomme, P. Blanchard, S. Herreyre, K. Nechev, and R. J. Staniewicz, *J. Power Sources*, **146**, 90 (2005).
3. M. Wohlfahrt-Mehrens, C. Vogler, and J. Garche, *J. Power Sources*, **127**, 58 (2004).
4. J. Vetter, P. Novák, M. R. Wagner, C. Veit, K.-C. Möller, J. O. Besenhard, M. Winter, M. Wohlfahrt-Mehrens, C. Vogler, and A. Hammouche, *J. Power Sources*, **147**, 269 (2005).
5. T. Waldmann, S. Gorse, T. Samtleben, G. Schneider, V. Knoblauch, and M. Wohlfahrt-Mehrens, *J. Electrochem. Soc.*, **161**, A1742 (2014).
6. S. Gorse, B. Kugler, T. Samtleben, T. Waldmann, M. Wohlfahrt-Mehrens, G. Schneider, and V. Knoblauch, *Pract. Metallogr.*, **51**, 829 (2014).
7. T. Waldmann et al., *J. Electrochem. Soc.*, **163**, A2149 (2016).
8. T. Waldmann, B.-I. Hogg, and M. Wohlfahrt-Mehrens, *J. Power Sources*, **384**, 107 (2018).
9. M. Dubarry, N. Qin, and P. Brooker, *Curr. Opin. Electrochem.*, **9**, 106 (2018).
10. M. Weiss et al., *Adv. Energy Mater.*, **11**, 2101126 (2021).
11. T. Waldmann, M. Wilka, M. Kasper, M. Fleischhammer, and M. Wohlfahrt-Mehrens, *J. Power Sources*, **262**, 129 (2014).
12. T. Waldmann, N. Ghanbari, M. Kasper, and M. Wohlfahrt-Mehrens, *J. Electrochem. Soc.*, **162**, A1500 (2015).
13. N. Paul, J. Keil, F. M. Kindermann, S. Schebesta, O. Dolotko, M. J. Mühlbauer, L. Kraft, S. V. Erhard, A. Jossen, and R. Gilles, *J. Energy Storage*, **17**, 383 (2018).
14. N. Paul, J. Wandt, S. Seidlmayer, S. Schebesta, M. J. Mühlbauer, O. Dolotko, H. A. Gasteiger, and R. Gilles, *J. Power Sources*, **345**, 85 (2017).
15. J. Keil, N. Paul, V. Baran, P. Keil, R. Gilles, and A. Jossen, *J. Electrochem. Soc.*, **166**, A3908 (2019).
16. K. Richter, T. Waldmann, M. Kasper, C. Pfeifer, M. Memm, P. Axmann, and M. Wohlfahrt-Mehrens, *J. Phys. Chem. C*, **123**, 18795 (2019).
17. K. Richter, T. Waldmann, N. Paul, N. Jobst, R. Scurtu, M. Hofmann, R. Gilles, and M. Wohlfahrt-Mehrens, *ChemSusChem*, **13**, 529 (2020).
18. M. Flügel, K. Richter, M. Wohlfahrt-Mehrens, and T. Waldmann, *J. Electrochem. Soc.*, **169**, 050533 (2022).
19. I. Zilberman, J. Sturm, and A. Jossen, *J. Power Sources*, **425**, 217 (2019).
20. J. D. McBrayer et al., *Nat. Energy*, **6**, 866 (2021).
21. N. Paul, H. Frielinghaus, S. Busch, V. Pipich, and R. Gilles, *J. Surf. Investig. X-Ray Synchrotron Neutron Tech.*, **14**, S156 (2020).
22. N. Paul, M. Wetjen, S. Busch, H. Gasteiger, and R. Gilles, *J. Electrochem. Soc.*, **166**, A1051 (2019).
23. B. Stiaszny, J. C. Ziegler, E. E. Krauß, J. P. Schmidt, and E. Ivers-Tiffée, *J. Power Sources*, **251**, 439 (2014).
24. J. A. Gilbert, I. A. Shkrob, and D. P. Abraham, *J. Electrochem. Soc.*, **164**, A389 (2017).
25. M. Börner, S. Klamor, B. Hoffmann, M. Schroeder, S. Nowak, A. Würsig, M. Winter, and F. M. Schappacher, *J. Electrochem. Soc.*, **163**, A831 (2016).
26. I. Buchberger, S. Seidlmayer, A. Pokharel, M. Piana, J. Hattendorff, P. Kudejova, R. Gilles, and H. A. Gasteiger, *J. Electrochem. Soc.*, **162**, A2737 (2015).
27. X. Fleury, M. H. Noh, S. Geniès, P. X. Thivel, C. Lefrou, and Y. Bultel, *J. Energy Storage*, **16**, 21 (2018).
28. A. Pfrang, A. Kersys, A. Kriston, D. U. Sauer, C. Rahe, S. Käbitz, and E. Figgemeier, *J. Power Sources*, **392**, 168 (2018).
29. C. Weisenberger, B. Meir, S. Röhrler, D. K. Harrison, and V. Knoblauch, *Electrochim. Acta*, **379**, 138145 (2021).
30. L. K. Willenberg, P. Dechent, G. Fuchs, D. U. Sauer, and E. Figgemeier, *Sustainability*, **12**, 557 (2020).
31. L. Willenberg, P. Dechent, G. Fuchs, M. Teuber, M. Eckert, M. Graff, N. Kürten, D. U. Sauer, and E. Figgemeier, *J. Electrochem. Soc.*, **167**, 120502 (2020).
32. T. Waldmann, R.-G. Scurtu, D. Brändle, and M. Wohlfahrt-Mehrens, *Energy Technol.*, **11**, 2200583 (2022).
33. J. C. Burns, D. A. Stevens, and J. R. Dahn, *J. Electrochem. Soc.*, **162**, A959 (2015).
34. T. Waldmann, B.-I. Hogg, M. Kasper, S. Grolleau, C. G. Couceiro, K. Trad, B. P. Matadi, and M. Wohlfahrt-Mehrens, *J. Electrochem. Soc.*, **163**, A1232 (2016).
35. M. Flügel, M. Bolsinger, M. Marinaro, V. Knoblauch, M. Hölzle, M. Wohlfahrt-Mehrens, and T. Waldmann, *J. Electrochem. Soc.*, **170**, 060536 (2023).
36. N. Ghanbari, T. Waldmann, M. Kasper, P. Axmann, and M. Wohlfahrt-Mehrens, *J. Phys. Chem. C*, **120**, 22225 (2016).
37. G. Kucinskis, M. Bozorgchenani, M. Feinauer, M. Kasper, M. Wohlfahrt-Mehrens, and T. Waldmann, *J. Power Sources*, **549**, 232129 (2022).
38. M. Bozorgchenani, G. Kucinskis, M. Wohlfahrt-Mehrens, and T. Waldmann, *J. Electrochem. Soc.*, **169**, 030509 (2022).
39. X.-G. Yang and C.-Y. Wang, *J. Power Sources*, **402**, 489 (2018).

40. B.-I. Hogg, T. Waldmann, and M. Wohlfahrt-Mehrens, *J. Electrochem. Soc.*, **167**, 090525 (2020).
41. D. Anseán, M. D Barry, A. Devie, B. Y. Liaw, V. M. García, J. C. Viera, and M. González, *J. Power Sources*, **356**, 36 (2017).
42. T. C. Bach, S. F. Schuster, E. Fleder, J. Müller, M. J. Brand, H. Lorrmann, A. Jossen, and G. SEXTL, *J. Energy Storage*, **5**, 212 (2016).
43. R. Carter and C. T. Love, *ACS Appl. Mater. Interfaces*, **10**, 26328 (2018).
44. M. Ecker, P. Shafiei Sabet, and D. U. Sauer, *Appl. Energy*, **206**, 934 (2017).
45. T. Waldmann, M. Kasper, and M. Wohlfahrt-Mehrens, *Electrochim. Acta*, **178**, 525 (2015).
46. T. Waldmann and M. Wohlfahrt-Mehrens, *Electrochim. Acta*, **230**, 454 (2017).
47. T. Waldmann, J. B. Quinn, K. Richter, M. Kasper, A. Tost, A. Klein, and M. Wohlfahrt-Mehrens, *J. Electrochem. Soc.*, **164**, A3154 (2017).
48. M. Fleischhammer, T. Waldmann, G. Bisle, B.-I. Hogg, and M. Wohlfahrt-Mehrens, *J. Power Sources*, **274**, 432 (2015).
49. A. A. Abd-El-Latif, P. Sichler, M. Kasper, T. Waldmann, and M. Wohlfahrt-Mehrens, *Batter. Supercaps*, **4**, 1135 (2021).
50. M. Feinauer, A. A. Abd-El-Latif, P. Sichler, A. Aracil Regalado, M. Wohlfahrt-Mehrens, and T. Waldmann, *J. Power Sources*, **570**, 233046 (2023).
51. Y. Preger, L. Torres-Castro, T. Rauhala, and J. Jeevarajan, *J. Electrochem. Soc.*, **169**, 030507 (2022).
52. M. Petzl and M. A. Danzer, *J. Power Sources*, **254**, 80 (2014).
53. M. Petzl, M. Kasper, and M. A. Danzer, *J. Power Sources*, **275**, 799 (2015).
54. B. Bitzer and A. Gruhle, *J. Power Sources*, **262**, 297 (2014).
55. V. Zinth, C. von Lüders, M. Hofmann, J. Hattendorff, I. Buchberger, S. Erhard, J. Rebelo-Kornmeier, A. Jossen, and R. Gilles, *J. Power Sources*, **271**, 152 (2014).
56. C. von Lüders, V. Zinth, S. V. Erhard, P. J. Osswald, M. Hofmann, R. Gilles, and A. Jossen, *J. Power Sources*, **342**, 17 (2017).
57. H.-P. Lin, D. Chua, M. Salomon, H.-C. Shiao, M. Hendrickson, E. Plichta, and S. Slane, *Electrochem. Solid-State Lett.*, **4**, A71 (2001).
58. P. M. Attia et al., *J. Electrochem. Soc.*, **169**, 060517 (2022).
59. X.-G. Yang, Y. Leng, G. Zhang, S. Ge, and C.-Y. Wang, *J. Power Sources*, **360**, 28 (2017).
60. L. E. Downie, L. J. Krause, J. C. Burns, L. D. Jensen, V. L. Chevrier, and J. R. Dahn, *J. Electrochem. Soc.*, **160**, A588 (2013).
61. M. C. Smart and B. V. Ratnakumar, *J. Electrochem. Soc.*, **158**, A379 (2011).
62. C. Uhlmann, J. Illig, M. Ender, R. Schuster, and E. Ivers-Tiffée, *J. Power Sources*, **279**, 428 (2015).
63. S. Schindler, M. Bauer, M. Petzl, and M. A. Danzer, *J. Power Sources*, **304**, 170 (2016).
64. M. Bauer, M. Wachtler, H. Stöwe, J. V. Persson, and M. A. Danzer, *J. Power Sources*, **317**, 93 (2016).
65. A. Friesen, F. Horsthemke, X. Mönninghoff, G. Brunklaus, R. Krafft, M. Börner, T. Risthaus, M. Winter, and F. M. Schappacher, *J. Power Sources*, **334**, 1 (2016).
66. H. Onbo, K. Takei, Y. Ishii, and T. Nishida, *J. Power Sources*, **189**, 337 (2009).
67. M. Zier, F. Scheiba, S. Oswald, J. Thomas, D. Goers, T. Scherer, M. Klose, H. Ehrenberg, and J. Eckert, *J. Power Sources*, **266**, 198 (2014).
68. C. Hogrefe, T. Waldmann, M. Hölzle, and M. Wohlfahrt-Mehrens, *J. Power Sources*, **556**, 232391 (2023).
69. P. P. Paul et al., *Adv. Energy Mater.*, **11**, 2100372 (2021).
70. I. D. Campbell, M. Marzook, M. Marinescu, and G. J. Offer, *J. Electrochem. Soc.*, **166**, A725 (2019).
71. J. Fan and S. Tan, *J. Electrochem. Soc.*, **153**, A1081 (2006).
72. C. Fear, T. Adhikary, R. Carter, A. N. Mistry, C. T. Love, and P. P. Mukherjee, *ACS Appl. Mater. Interfaces*, **12**, 30438 (2020).
73. J. E. Harlow, S. L. Glazier, J. Li, and J. R. Dahn, *J. Electrochem. Soc.*, **165**, A3595 (2018).
74. Z. M. Konz, E. J. McShane, and B. D. McCloskey, *ACS Energy Lett.*, **5**, 1750 (2020).
75. U. Janakiraman, T. R. Garrick, and M. E. Fortier, *J. Electrochem. Soc.*, **167**, 160552 (2020).
76. N. Ghanbari, T. Waldmann, M. Kasper, P. Axmann, and M. Wohlfahrt-Mehrens, *ECS Electrochem. Lett.*, **4**, A100 (2015).
77. M. Börner, A. Friesen, M. Grütze, Y. P. Stenzel, G. Brunklaus, J. Haetge, S. Nowak, F. M. Schappacher, and M. Winter, *J. Power Sources*, **342**, 382 (2016).
78. A. Iturrodoibeitia, F. Aguesse, S. Genies, T. Waldmann, M. Kasper, N. Ghanbari, M. Wohlfahrt-Mehrens, and E. Bekaert, *J. Phys. Chem. C*, **121**, 21865 (2017).
79. Y. Krämer, C. Birkenmaier, J. Feinauer, A. Hintennach, C. L. Bender, M. Meiler, V. Schmidt, R. E. Dinneber, and T. Schleid, *Chem. - Eur. J.*, **21**, 6062 (2015).
80. B. P. Matadi et al., *J. Electrochem. Soc.*, **164**, A1089 (2017).
81. J. Arai, Y. Okada, T. Sugiyama, M. Izuka, K. Gotoh, and K. Takeda, *J. Electrochem. Soc.*, **162**, A952 (2015).
82. T. Gao, Y. Han, D. Fraggadakis, S. Das, T. Zhou, C.-N. Yeh, S. Xu, W. C. Chueh, J. Li, and M. Z. Bazant, *Joule*, **5**, 393 (2021).
83. S. A. Kayser, A. Mester, A. Mertens, P. Jakes, R.-A. Eichel, and J. Granwehr, *Phys. Chem. Chem. Phys.*, **20**, 13765 (2018).
84. D. Wasylowski, S. Neubauer, M. Faber, H. Dittler, M. Sonnet, A. Blömeke, P. Dechent, A. Gitis, and D. U. Sauer, *J. Power Sources*, **580**, 233295 (2023).
85. J.-H. Cheng, A. A. Assegie, C.-J. Huang, M.-H. Lin, A. M. Tripathi, C.-C. Wang, M.-T. Tang, Y.-F. Song, W.-N. Su, and B. J. Hwang, *J. Phys. Chem. C*, **121**, 7761 (2017).
86. S. Hein and A. Latz, *Electrochim. Acta*, **201**, 354 (2016).
87. S. Hein and A. Latz, *ECS Trans.*, **69**, 3 (2015).
88. S. Hein, T. Danner, and A. Latz, *ACS Appl. Energy Mater.*, **3**, 8519 (2020).
89. X. Lu et al., *Nat. Commun.*, **14**, 5127 (2023).
90. S. Carelli and W. G. Bessler, *J. Electrochem. Soc.*, **167**, 100515 (2020).
91. T. Sun et al., *Electrochim. Acta*, **425**, 140701 (2022).
92. V. Kabra, M. Parmananda, C. Fear, F. L.-E. Usseglio-Viretta, A. Colclasure, K. Smith, and P. P. Mukherjee, *ACS Appl. Mater. Interfaces*, **12**, 55795 (2020).
93. S. Tippmann, D. Walper, L. Balboa, B. Spier, and W. G. Bessler, *J. Power Sources*, **252**, 305 (2014).
94. J. Remmlinger, S. Tippmann, M. Buchholz, and K. Dietmayer, *J. Power Sources*, **254**, 268 (2014).
95. M. Tang, P. Albertus, and J. Newman, *J. Electrochem. Soc.*, **156**, A390 (2009).
96. Y. Pan, X. Han, X. Kong, L. Lu, M. Ouyang, J. Zhang, Y. Wang, and H. Zheng, *J. Energy Storage*, **73**, 109176 (2023).
97. Z. He, H. Li, W. Ji, W. Li, Y. Zhang, X. Li, P. Zhang, and J. Zhao, *J. Power Sources*, **571**, 233044 (2023).
98. F. Brosa Planella and W. D. Widanage, *Appl. Math. Model.*, **121**, 586 (2023).
99. C.-H. Chen, F. Brosa Planella, K. O'Regan, D. Gastol, W. D. Widanage, and E. Kendrick, *J. Electrochem. Soc.*, **167**, 080534 (2020).
100. P. Brodsky Ringler, M. Wise, P. Ramesh, J. H. Kim, M. Canova, C. Bae, J. Deng, and H. Park, *Batteries*, **9**, 337 (2023).
101. P. Arora, M. Doyle, and R. E. White, *J. Electrochem. Soc.*, **146**, 3543 (1999).
102. C. von Lüders, J. Keil, M. Webersberger, and A. Jossen, *J. Power Sources*, **414**, 41 (2019).
103. A. S. Mijailovic, G. Wang, Y. Li, J. Yang, W. Lu, Q. Wu, and B. W. Sheldon, *J. Electrochem. Soc.*, **169**, 060529 (2022).
104. A. S. Mijailovic, G. Wang, M. Luo, W. Lu, Q. Wu, and B. W. Sheldon, *J. Electrochem. Soc.*, **170**, 070508 (2023).
105. N. Legrand, B. Knosp, P. Desprez, F. Lapique, and S. Raël, *J. Power Sources*, **245**, 208 (2014).
106. S. Sahu and J. M. Foster, *J. Energy Storage*, **60**, 106516 (2023).
107. D. R. Baker and M. W. Verbrugge, *J. Electrochem. Soc.*, **167**, 013504 (2020).
108. D. Gaissmaier, D. Fantauzzi, and T. Jacob, *J. Chem. Phys.*, **150**, 041723 (2019).
109. M. Jäckle and A. Groß, *J. Chem. Phys.*, **141**, 174710 (2014).
110. M. Jäckle, K. Helmbrecht, M. Smits, D. Stottmeister, and A. Groß, *Energy Environ. Sci.*, **11**, 3400 (2018).
111. J. Yu and R. Buyya, *J. Grid Comput.*, **3**, 171 (2005).
112. <https://dictionary.cambridge.org/dictionary/english/workflow> (09.07.2024).
113. I. Pivarníková, M. Flügel, N. Paul, A. Cannavo, G. Ceccio, J. Vacík, P. Müller-Buschbaum, M. Wohlfahrt-Mehrens, R. Gilles, and T. Waldmann, *J. Power Sources*, **594**, 233972 (2024).
114. U. R. Koletti, C. Zhang, R. Malik, T. Q. Dinh, and J. Marco, *J. Energy Storage*, **24**, 100798 (2019).
115. A. Adam, K. Huber, E. Knobbe, D. Griebl, J. Wandt, and A. Kwade, *J. Power Sources*, **512**, 230469 (2021).
116. V. Zinth, C. von Lüders, J. Wilhelm, S. V. Erhard, M. Hofmann, S. Seidlmayer, J. Rebelo-Kornmeier, W. Gan, A. Jossen, and R. Gilles, *J. Power Sources*, **361**, 54 (2017).
117. C. Hogrefe, S. Hein, T. Waldmann, T. Danner, K. Richter, A. Latz, and M. Wohlfahrt-Mehrens, *J. Electrochem. Soc.*, **167**, 140546 (2020).
118. F. Buchner, J. Kim, C. Adler, M. Bozorgchenani, J. Bansmann, and R. J. Behm, *J. Phys. Chem. Lett.*, **8**, 5804 (2017).
119. M. T. Johnson, H. I. Starnberg, and H. P. Hughes, *Surf. Sci.*, **178**, 290 (1986).
120. Z. P. Hu and A. Ignatiev, *Phys. Rev. B*, **30**, 4856 (1984).
121. F. Holtstiege, R. Schmuch, M. Winter, G. Brunklaus, and T. Placke, *J. Power Sources*, **378**, 522 (2018).
122. A. Shalikeri, V. G. Watson, D. L. Adams, E. E. Kalu, J. A. Read, T. R. Jow, and J. P. Zheng, *ECS Trans.*, **77**, 293 (2017).
123. L. Mandeltort and J. T. Yates, *J. Phys. Chem. C*, **116**, 24962 (2012).
124. F. Yao, F. Güneş, H. Q. Ta, S. M. Lee, S. J. Chae, K. Y. Sheem, C. S. Cojocaru, S. S. Xie, and Y. H. Lee, *J. Am. Chem. Soc.*, **134**, 8646 (2012).
125. C. Uthaisar and V. Barone, *Nano Lett.*, **10**, 2838 (2010).
126. X. Fan, W. T. Zheng, and J.-L. Kuo, *ACS Appl. Mater. Interfaces*, **4**, 2432 (2012).
127. L. Somerville, J. Baréño, P. Jennings, A. McGordon, C. Lyness, and I. Bloom, *Electrochim. Acta*, **206**, 70 (2016).
128. Y. Kobayashi, T. Kobayashi, K. Shono, Y. Ohno, Y. Mita, and H. Miyashiro, *J. Electrochem. Soc.*, **160**, A1181 (2013).
129. M. Klett, R. Eriksson, J. Groot, P. Svens, K. C. Högström, R. W. Lindström, H. Berg, T. Gustafson, G. Lindbergh, and K. Edström, *J. Power Sources*, **257**, 126 (2014).
130. K. Jalkanen, J. Karppinen, L. Skogström, T. Laurila, M. Nisula, and K. Vuoriolehto, *Appl. Energy*, **154**, 160 (2015).
131. H. Takahara, Y. Kobayashi, K. Shono, H. Kobayashi, M. Shikano, and T. Nakamura, *J. Electrochem. Soc.*, **161**, A1716 (2014).
132. M. Kassem and C. Delacourt, *J. Power Sources*, **235**, 159 (2013).
133. G. Kilibarda, S. Schlabach, V. Winkler, M. Bruns, T. Hanemann, and D. V. Szabó, *J. Power Sources*, **263**, 145 (2014).
134. H.-Y. Amanieu, D. Rosato, M. Sebastiani, F. Massimi, and D. C. Lupascu, *Mater. Sci. Eng. A*, **593**, 92 (2014).
135. A. Hightower, C. C. Ahn, B. Fultz, and P. Rez, *Appl. Phys. Lett.*, **77**, 238 (2000).
136. K. Kleiner, J. Melke, M. Merz, P. Jakes, P. Nagel, S. Schuppler, V. Liebau, and H. Ehrenberg, *ACS Appl. Mater. Interfaces*, **7**, 19589 (2015).
137. D. Aurbach, B. Markovsky, A. Rodkin, M. Cojocaru, E. Levi, and H.-J. Kim, *Electrochim. Acta*, **47**, 1899 (2002).
138. M. Bauer, C. Guenther, M. Kasper, M. Petzl, and M. A. Danzer, *J. Power Sources*, **283**, 494 (2015).
139. C. H. Hamann, A. Hamnett, and W. Vielstich, *Electrochemistry 2.*, completely rev. and updated ed., p. 531 (Wiley-VCH, Weinheim) (2007).
140. J. Steiger, D. Kramer, and R. Mönig, *J. Power Sources*, **261**, 112 (2014).
141. J. Steiger, D. Kramer, and R. Mönig, *Electrochim. Acta*, **136**, 529 (2014).

142. S. J. Harris, A. Timmons, D. R. Baker, and C. Monroe, *Chem. Phys. Lett.*, **485**, 265 (2010).
143. O. Crowther and A. C. West, *J. Electrochem. Soc.*, **155**, A806 (2008).
144. C. Brissot, M. Rosso, J.-N. Chazalviel, P. Baudry, and S. Lascaud, *Electrochim. Acta*, **43**, 1569 (1998).
145. F. Orsini, A. Du Pasquier, B. Beaudoin, J. M. Tarascon, M. Trentin, N. Langenhuizen, E. De Beer, and P. Notten, *J. Power Sources*, **76**, 19 (1998).
146. E. Santos and W. Schmickler, *Angew. Chem. Int. Ed.*, **60**, 5876 (2021).
147. C. T. Love, O. A. Baturina, and K. E. Swider-Lyons, *ECS Electrochem. Lett.*, **4**, A24 (2015).
148. S.-K. Otto, Y. Moryson, T. Krauskopf, K. Peppeler, J. Sann, J. Janek, and A. Henss, *Chem. Mater.*, **33**, 859 (2021).
149. S.-K. Otto, T. Fuchs, Y. Moryson, C. Lerch, B. Mogwitz, J. Sann, J. Janek, and A. Henss, *ACS Appl. Energy Mater.*, **4**, 12798 (2021).
150. P. Hovington, V. Timoshevskii, S. Burgess, H. Demers, P. Statham, R. Gauvin, and K. Zaghib, *Scanning*, **38**, 571 (2016).
151. J. A. Österreicher, C. Simson, A. Großalber, S. Frank, and S. Gneirer, *Scr. Mater.*, **194**, 113664 (2021).
152. U. Golla-Schindler, E. Barbosa Sa, C. Weisenberger, V. Knoblauch, and G. Schneider, *Microsc. Microanal.*, **29**, 117 (2023).
153. T. Sedlatschek, J. Lian, W. Li, M. Jiang, T. Wierzbicki, M. Z. Bazant, and J. Zhu, *Acta Mater.*, **208**, 116730 (2021).
154. T. Fuchs, C. G. Haslam, A. C. Moy, C. Lerch, T. Krauskopf, J. Sakamoto, F. H. Richter, and J. Janek, *Adv. Energy Mater.*, **12**, 2201125 (2022).
155. R. Gilles, *J. Surf. Investig. X-Ray Synchrotron Neutron Tech.*, **14**, S69 (2020).
156. H. J. Chang, N. M. Trease, A. J. Iliot, D. Zeng, L.-S. Du, A. Jerschow, and C. P. Grey, *J. Phys. Chem. C*, **119**, 16443 (2015).
157. Y.-C. Hsieh, M. Leiβing, S. Nowak, B.-J. Hwang, M. Winter, and G. Brunklaus, *Cell Rep. Phys. Sci.*, **1**, 100139 (2020).
158. B. Rieger, S. F. Schuster, S. V. Erhard, P. J. Osswald, A. Rheinfeld, C. Willmann, and A. Jossen, *J. Energy Storage*, **8**, 1 (2016).
159. C. Bommier, W. Chang, Y. Lu, J. Yeung, G. Davies, R. Mohr, M. Williams, and D. Steingart, *Cell Rep. Phys. Sci.*, **1**, 100035 (2020).
160. H. Takahara, M. Shikano, and H. Kobayashi, *J. Power Sources*, **244**, 252 (2013).
161. H. Takahara, H. Miyauchi, M. Tabuchi, and T. Nakamura, *J. Electrochem. Soc.*, **160**, A272 (2013).
162. G. Carbonari, R.-G. Scurtu, T. Waldmann, S. Radloff, M. Flügel, A. Hoffmann, and M. Wohlfahrt-Mehrens, *J. Electrochem. Soc.*, **168**, 050508 (2021).
163. M. Flügel, T. Waldmann, M. Kasper, and M. Wohlfahrt-Mehrens, *ChemPhysChem*, **21**, 2047 (2020).
164. M. Flügel, M. Kasper, C. Pfeifer, M. Wohlfahrt-Mehrens, and T. Waldmann, *J. Electrochem. Soc.*, **168**, 020506 (2021).
165. Y. Saito and M.-K. Rahman, *J. Power Sources*, **174**, 877 (2007).
166. H. Takahara, A. Kojo, K. Kodama, T. Nakamura, K. Shono, Y. Kobayashi, M. Shikano, and H. Kobayashi, *J. Anal. At. Spectrom.*, **29**, 95 (2014).
167. T. Nelis and R. Payling, *Glow Discharge Optical Emission Spectroscopy: A Practical Guide* (Royal Society of Chemistry, Cambridge) (2003).
168. M. Trunk, M. Wetjen, L. Werner, R. Gernhäuser, B. Märkisch, Z. Révay, H. A. Gasteiger, and R. Gilles, *Mater. Charact.*, **146**, 127 (2018).
169. R. G. Downing, G. P. Lamaze, J. K. Langland, and S. T. Hwang, *J. Res. Natl. Inst. Stand. Technol.*, **98**, 109 (1993).
170. S. Whitney, S. R. Biegalski, Y. H. Huang, and J. B. Goodenough, *J. Electrochem. Soc.*, **156**, A886 (2009).
171. D. J. Lyons, J. L. Weaver, and A. C. Co, *J. Mater. Chem. A*, **10**, 2336 (2022).
172. M. Wetjen, M. Trunk, L. Werner, H. A. Gasteiger, R. Gernhäuser, R. Gilles, B. Märkisch, and Z. Révay, *J. Electrochem. Soc.*, **166**, A1408 (2019).
173. M. Wetjen, M. Trunk, L. Werner, R. Gernhäuser, B. Märkisch, Z. Révay, R. Gilles, and H. A. Gasteiger, *J. Electrochem. Soc.*, **165**, A2340 (2018).
174. E. Moyassari, T. Roth, S. Kücher, C.-C. Chang, S.-C. Hou, F. B. Spingler, and A. Jossen, *J. Electrochem. Soc.*, **169**, 010504 (2022).
175. F. Linsenmann, M. Trunk, P. Rapp, L. Werner, R. Gernhäuser, R. Gilles, B. Märkisch, Z. Révay, and H. A. Gasteiger, *J. Electrochem. Soc.*, **167**, 100554 (2020).
176. I. Tomandl et al., *Radiat. Eff. Defects Solids*, **175**, 394 (2020).
177. L. Kong, Y. Xing, and M. G. Pecht, *IEEE Access*, **6**, 8387 (2018).
178. C. Hogrefe, T. Waldmann, M. B. Molinero, L. Wildner, P. Axmann, and M. Wohlfahrt-Mehrens, *J. Electrochem. Soc.*, **169**, 050519 (2022).
179. Z. Guo, J. Zhu, J. Feng, and S. Du, *RSC Adv.*, **5**, 69514 (2015).
180. P. Maire, A. Evans, H. Kaiser, W. Scheifele, and P. Novák, *J. Electrochem. Soc.*, **155**, A862 (2008).
181. C. Hogrefe, M. Hölzle, M. Wohlfahrt-Mehrens, and T. Waldmann, *J. Electrochem. Soc.*, **170**, 110535 (2023).
182. R. Juza and V. Wehle, *Naturwissenschaften*, **52**, 560560 (1965).
183. K. C. Woo, W. A. Kamitakahara, D. P. DiVincenzo, D. S. Robinson, H. Mertwoy, J. W. Milliken, and J. E. Fischer, *Phys. Rev. Lett.*, **50**, 182 (1983).
184. E. Abbe, *Arch. Für Mikrosk. Anat.*, **9**, 413 (1873).
185. T. Bernthaler, T. Schubert, and C. Weisenberger, *Optische Inspektion: Mikroskopische Mess- und Analyseverfahren in der Industrie* p. 70 (Verl. Moderne Industrie, Landsberg) (2014).
186. R. G. Lerner and G. L. Trigg, *Encyclopedia of physics* 3rd ed. ed., completely rev. and enl., p. 2 (Wiley-VCH, Weinheim) (2005).
187. J. I. Goldstein, D. E. Newbury, J. R. Michael, N. W.-M. Ritchie, J. H.-J. Scott, and D. C. Joy, *Scanning Electron Microscopy and X-ray Microanalysis* (Springer New York, New York, NY) (2018), <https://link.springer.com/10.1007/978-1-4939-6676-9>.
188. V.-D. Hodoroaba, *Characterization of Nanoparticles* p. 397 (Elsevier, Amsterdam) (2020), <https://linkinghub.elsevier.com/retrieve/pii/B9780128141823000213>.
189. L. Xiaobing, J. Holland, S. Burgess, S. Bhadare, S. Yamaguchi, D. Birtwistle, P. Statham, and N. Rowlands, *Microsc. Microanal.*, **19**, 1136 (2013).
190. K. Yan, Z. Lu, H.-W. Lee, F. Xiong, P.-C. Hsu, Y. Li, J. Zhao, S. Chu, and Y. Cui, *Nat. Energy*, **1**, 16010 (2016).
191. R. Raccichini, M. Amores, and G. Hinds, *Batteries*, **5**, 12 (2019).
192. S. E.-J. O'Kane, W. Ai, G. Madabattula, D. Alonso-Alvarez, R. Timms, V. Sulzer, J. S. Edge, B. Wu, G. J. Offer, and M. Marinescu, *Phys. Chem. Chem. Phys.*, **24**, 7909 (2022).
193. S. Ding, Y. Li, H. Dai, L. Wang, and X. He, *Adv. Energy Mater.*, **13**, 2301452 (2023).
194. Y. Takagishi and T. Yamaue, *J. Electrochem. Soc.*, **170**, 030528 (2023).
195. M. Feinauer, M. Wohlfahrt-Mehrens, M. Hölzle, and T. Waldmann, *J. Power Sources*, **594**, 233948 (2024).
196. L. Werner, M. Trunk, R. Gernhäuser, R. Gilles, B. Märkisch, and Z. Révay, *Nucl. Instrum. Methods Phys. Res. Sect. Accel. Spectrometers Detect. Assoc. Equip.*, **911**, 30 (2018).
197. M. Frankenberger et al., *Batteries*, **6**, 21 (2020).
198. E. Moyassari, L. Streck, N. Paul, M. Trunk, R. Neagu, C.-C. Chang, S.-C. Hou, B. Märkisch, R. Gilles, and A. Jossen, *J. Electrochem. Soc.*, **168**, 020519 (2021).
199. C. E. Hendricks, A. N. Mansour, D. A. Fuentevilla, G. H. Waller, J. K. Ko, and M. G. Pecht, *J. Electrochem. Soc.*, **167**, 090501 (2020).
200. J. Kasnatscheew, M. Börner, B. Streipert, P. Meister, R. Wagner, I. Cekic Laskovic, and M. Winter, *J. Power Sources*, **362**, 278 (2017).
201. C. Fear, D. Juarez-Robles, J. A. Jeevarajan, and P. P. Mukherjee, *J. Electrochem. Soc.*, **165**, A1639 (2018).
202. R. Guo, L. Lu, M. Ouyang, and X. Feng, *Sci. Rep.*, **6** (2016), <http://nature.com/articles/srep30248>.
203. S. Dayani, H. Markötter, J. von Krug von Nidda, A. Schmidt, and G. Bruno, *Adv. Mater. Technol.*, **9**, 2301246 (2023).
204. Y. Reynier, R. Yazami, and B. Fultz, *J. Power Sources*, **119–121**, 850 (2003).
205. T. Waldmann, G. Bisle, B.-I. Hogg, S. Stumpp, M. A. Danzer, M. Kasper, P. Axmann, and M. Wohlfahrt-Mehrens, *J. Electrochem. Soc.*, **162**, A921 (2015).
206. R. L. Sacci, L. W. Gill, E. W. Hagaman, and N. J. Dudney, *J. Power Sources*, **287**, 253 (2015).
207. J. Kuwabara and K. Sato, *ECS Trans.*, **75**, 47 (2017).
208. T. Langner, T. Sieber, and J. Acker, *Sci. Rep.*, **11**, 6316 (2021).
209. F. Grimsmann, T. Gerbert, F. Brauchle, A. Gruhle, J. Parisi, and M. Knipper, *J. Energy Storage*, **15**, 17 (2018).
210. C. Birkenmaier, B. Bitzer, M. Harzheim, A. Hintennach, and T. Schleid, *J. Electrochem. Soc.*, **162**, A2646 (2015).
211. J. Cannarella and C. B. Arnold, *J. Electrochem. Soc.*, **162**, A1365 (2015).
212. Y. Wu, S. Saxena, Y. Xing, Y. Wang, C. Li, W. Yung, and M. Pecht, *Energies*, **11**, 925 (2018).
213. R. Schäfer, E. Delz, M. Kasper, V. Knoblauch, M. Wohlfahrt-Mehrens, and T. Waldmann, *J. Electrochem. Soc.*, **170**, 120519 (2023).
214. A. S. Mussa, G. Lindbergh, M. Klett, P. Gudmundson, P. Svens, and R. W. Lindström, *J. Energy Storage*, **20**, 213 (2018).
215. T. Waldmann, R.-G. Scurtu, K. Richter, and M. Wohlfahrt-Mehrens, *J. Power Sources*, **472**, 228614 (2020).
216. T. Waldmann, S. Rössler, M. Blessing, R. Schäfer, R.-G. Scurtu, W. Braunwarth, and M. Wohlfahrt-Mehrens, *J. Electrochem. Soc.*, **168**, 090519 (2021).
217. B. Kellers, M. P. Lautenschlaeger, N. Rigos, J. Weinmiller, T. Danner, and A. Latz, *Batteries*, **9**, 390 (2023).
218. L. J. Bolay et al., *J. Power Sources Adv.*, **14**, 100083 (2022).
219. V. De Lauri, L. Krumbein, S. Hein, B. Prifling, V. Schmidt, T. Danner, and A. Latz, *ACS Appl. Energy Mater.*, **4**, 13847 (2021).
220. K. Persson, V. A. Sethuraman, L. J. Hardwick, Y. Hinuma, Y. S. Meng, A. van der Ven, V. Srinivasan, R. Kostecki, and G. Ceder, *J. Phys. Chem. Lett.*, **1**, 1176 (2010).
221. K. Persson, Y. Hinuma, Y. S. Meng, A. Van der Ven, and G. Ceder, *Phys. Rev. B*, **82** (2010), <https://doi.org/10.1103/PhysRevB.82.125416>.
222. Y. Guo, R. B. Smith, Z. Yu, D. K. Efetov, J. Wang, P. Kim, M. Z. Bazant, and L. E. Brus, *J. Phys. Chem. Lett.*, **7**, 2151 (2016).
223. X.-G. Yang, T. Liu, Y. Gao, S. Ge, Y. Leng, D. Wang, and C.-Y. Wang, *Joule*, **3**, 3002 (2019).
224. X.-G. Yang, G. Zhang, S. Ge, and C.-Y. Wang, *Proc. Natl. Acad. Sci.*, **115**, 7266 (2018).
225. T. Danner, M. Singh, S. Hein, J. Kaiser, H. Hahn, and A. Latz, *J. Power Sources*, **334**, 191 (2016).
226. B. P. Matadi, S. Genies, A. Delaille, C. Chabrol, E. de Vito, M. Bardet, J.-F. Martin, L. Daniel, and Y. Bultel, *J. Electrochem. Soc.*, **164**, A2374 (2017).
227. I. A. Shkrob, M.-T. F. Rodrigues, and D. P. Abraham, *J. Electrochem. Soc.*, **168**, 010512 (2021).
228. C. Mao, R. E. Ruther, J. Li, Z. Du, and I. Belharouak, *Electrochem. Commun.*, **97**, 37 (2018).
229. R. Nölle, K. Beltrop, F. Holtstiege, J. Kasnatscheew, T. Placke, and M. Winter, *Mater. Today*, **32**, 131 (2020).
230. S. Krueger, R. Kloepsch, J. Li, S. Nowak, S. Passerini, and M. Winter, *J. Electrochem. Soc.*, **160**, A542 (2013).
231. B. Michalak, B. B. Berkes, H. Sommer, T. Brezesinski, and J. Janek, *J. Phys. Chem. C*, **121**, 211 (2017).
232. Y. Kuhn, H. Wolf, A. Latz, and B. Horstmann, *Batteries & Supercaps*, **6**, e202200374 (2023).
233. R. V. Bugga and M. C. Smart, *ECS Transactions*, **25**, 241 (2010).
234. *Analytic Methods for Design Practice* G.-J. Park (ed.), (Springer London, London) p. 309 (2007).
235. S. Greenhill, S. Rana, S. Gupta, P. Vellanki, and S. Venkatesh, *IEEE Access*, **8**, 13937 (2020).